iScience

CellPress
OPEN ACCESS

Article

Actin crosslinking by α-actinin averts viscous dissipation of myosin force transmission in stress fibers

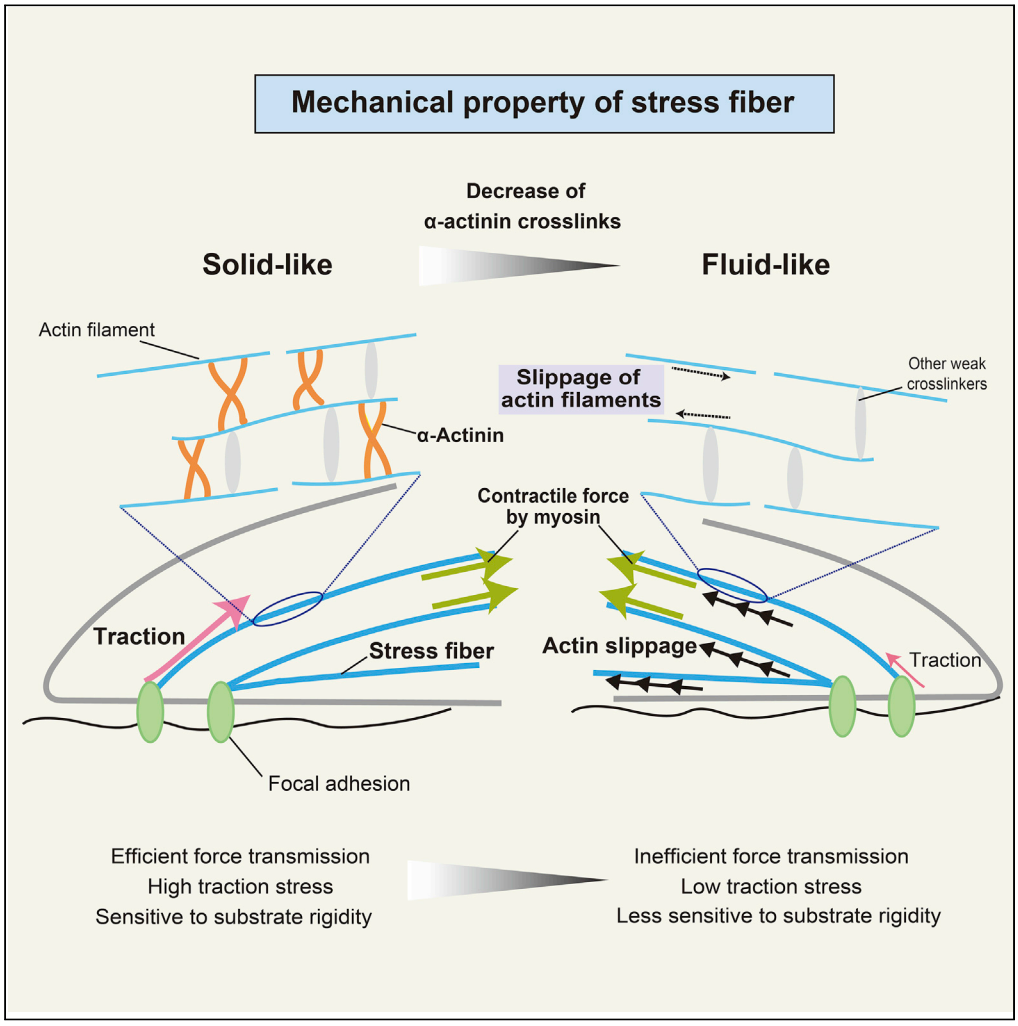

Hiroki Katsuta, Satoru Okuda, Kazuaki Nagayama, ..., Masahiro Sokabe, Takaki Miyata, Hiroaki Hirata

hirata@neptune.kanazawa-it.ac.jp

Highlights

Actin crosslinking by α-actinin solidifies stress fibers (SFs)

Inhibition of α-actinin crosslinking induces actin and myosin flows along SFs

SF fluidization diminishes transmission of myosin-generated force along SFs

α-Actinin is essential for rigidity-dependent regulation of cell migration speed

Katsuta et al., iScience 26, 106090
March 17, 2023
https://doi.org/10.1016/j.isci.2023.106090

iScience

CellPress
OPEN ACCESS

Article

Actin crosslinking by α-actinin averts viscous dissipation of myosin force transmission in stress fibers

Hiroki Katsuta,[1,2,3] Satoru Okuda,[4] Kazuaki Nagayama,[5] Hiroaki Machiyama,[6] Satoru Kidoaki,[7] Masashi Kato,[3] Masahiro Sokabe,[1,8] Takaki Miyata,[2] and Hiroaki Hirata[1,9,10,*]

SUMMARY

Contractile force generated in actomyosin stress fibers (SFs) is transmitted along SFs to the extracellular matrix (ECM), which contributes to cell migration and sensing of ECM rigidity. In this study, we show that efficient force transmission along SFs relies on actin crosslinking by α-actinin. Upon reduction of α-actinin-mediated crosslinks, the myosin II activity induced flows of actin filaments and myosin II along SFs, leading to a decrease in traction force exertion to ECM. The fluidized SFs maintained their cable integrity probably through enhanced actin polymerization throughout SFs. A computational modeling analysis suggested that lowering the density of actin crosslinks caused viscous slippage of actin filaments in SFs and, thereby, dissipated myosin-generated force transmitting along SFs. As a cellular scale outcome, α-actinin depletion attenuated the ECM-rigidity-dependent difference in cell migration speed, which suggested that α-actinin-modulated SF mechanics is involved in the cellular response to ECM rigidity.

INTRODUCTION

The actomyosin system serves as a major force generator in mammalian cells, contributing to cell migration,[1] cell differentiation,[2,3] cell division,[4–6] and muscle contraction.[7] Adherent cells form the actomyosin cables called stress fibers (SFs) whose tips are connected to focal adhesions (FAs), sites for cell adhesion to the extracellular matrix (ECM).[8,9] SFs generate a contractile force and transmit it along SFs to FAs,[10–14] which is essential for regulation of cell adhesion to ECM and cellular sensing of extracellular mechanical cues.[15] Molecular mechanisms for the regulation of contractile force generation have been extensively studied; phosphorylation of myosin regulatory light chain, which is regulated by myosin light-chain kinase, Rho kinase, and myosin light chain (MLC) phosphatase, activates non-muscle myosin II to induce ATP hydrolysis and force generation by myosin II.[16–18] From the mechanical point of view, SF acts not just as a passive elastic string but also as an active viscoelastic matter.[19–21] SFs are composed of sarcomere-like contractile units (CUs) in series that contain F-actin and myosin II; in each unit, 10–30 actin filaments are bundled by actin crosslinking proteins.[22–24] Akin to the case of crosslinked synthetic polymer networks, the viscoelastic property of the actin cytoskeleton is affected by actin crosslinkers; increasing the density of actin crosslinking proteins makes the actin cytoskeleton more elastic and solid-like.[25,26] While viscoelastic cytoskeletal networks exhibit non-linear behaviors in strain-stress relationship both *in vitro* and in cells,[27–29] it has been largely obscure how viscoelastic properties of SFs contribute to force transmission along SFs and cellular functions.

α-Actinin is a well-conserved and ubiquitously expressed actin crosslinking protein.[30–32] An α-actinin molecule consists of an actin-binding domain, a CaM-like domain, and a rod domain composed of four consecutive spectrin repeats and forms antiparallel homodimers.[33,34] Studies have shown that α-actinin is involved in SF maturation and mechanical resilience of the cytoskeleton network[35–37] and can serve as a molecular "shock absorber" in the actin cytoskeleton by changing folding states of its spectrin repeat domains in response to the cytoskeletal tension.[33] An increase in the affinity of α-actinin for actin has been shown to increase the elasticity of actin filament gels *in vitro*,[38] to reduce diffusive mobilities of cytoplasmic particles, suggesting solidification of the cytoplasmic environment in cells,[39] and to elevate cellular traction stress exerted to ECM.[39] Based on these results, Ehrlicher et al. discussed that α-actinin-mediated crosslinks of

[1]Mechanobiology Laboratory, Nagoya University Graduate School of Medicine, Nagoya 466-8550, Japan

[2]Anatomy and Cell Biology, Nagoya University Graduate School of Medicine, Nagoya 466-8550, Japan

[3]Department of Occupational and Environmental Health, Nagoya University Graduate School of Medicine, Nagoya 466-8550, Japan

[4]WPI Nano Life Science Institute, Kanazawa University, Kanazawa 920-1192, Japan

[5]Department of Mechanical Systems Engineering, Graduate School of Science and Engineering, Ibaraki University, Hitachi 316-8511, Japan

[6]Department of Immunology, Tokyo Medical University, Tokyo 160-8402, Japan

[7]Division of Applied Molecular Chemistry, Institute for Materials Chemistry and Engineering, Kyushu University, Fukuoka 819-0395, Japan

[8]Human Information Systems Laboratories, Kanazawa Institute of Technology, Hakusan 924-0838, Japan

[9]Department of Applied Bioscience, Kanazawa Institute of Technology, Hakusan 924-0838, Japan

[10]Lead contact

*Correspondence: hirata@neptune.kanazawa-it.ac.jp

https://doi.org/10.1016/j.isci.2023.106090

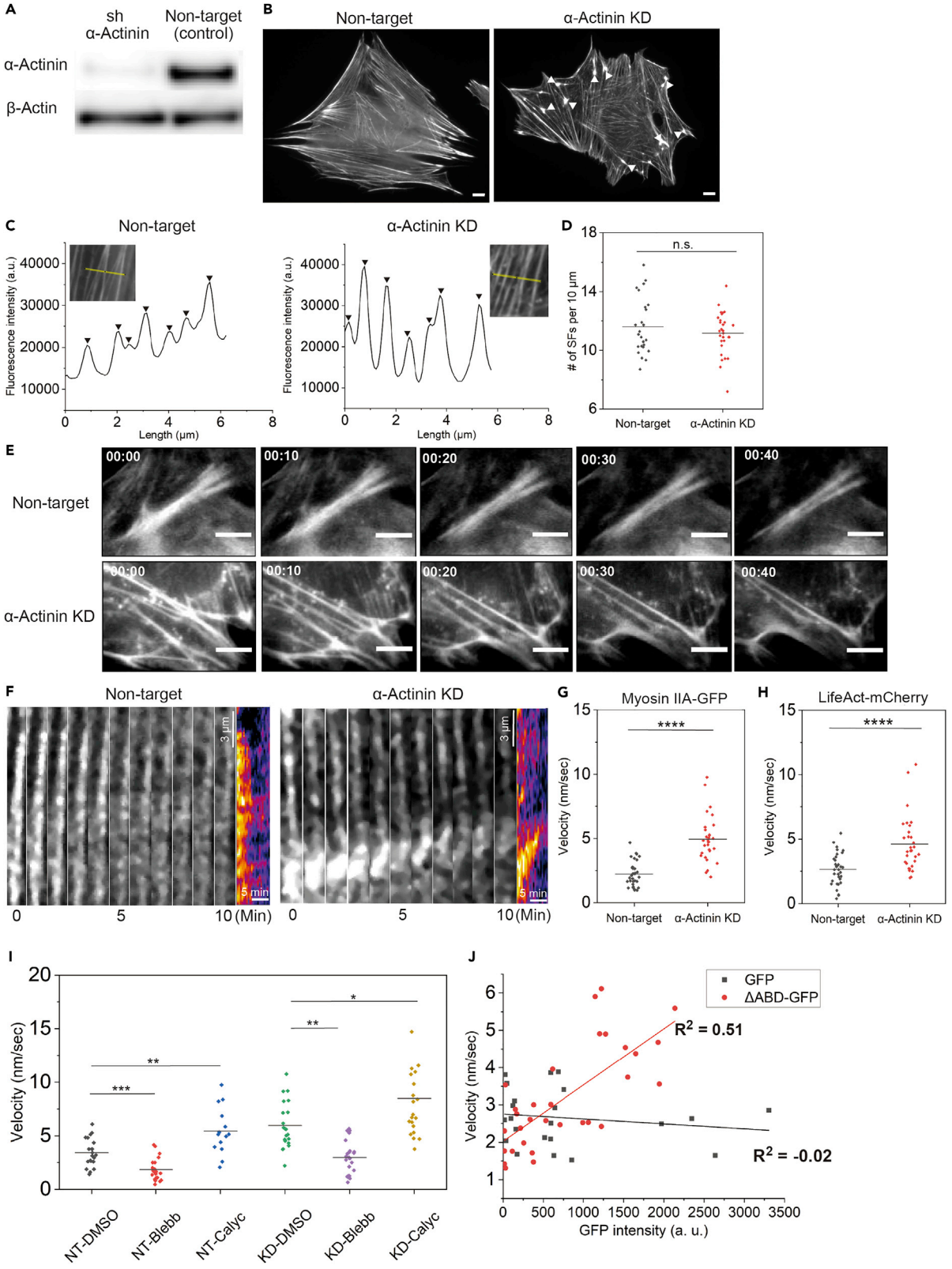
A
sh α-Actinin
Non-target (control)
α-Actinin
β-Actin
B
Non-target
α-Actinin KD
C
Non-target
α-Actinin KD
Fluorescence intensity (a.u.)
Length (μm)
D
n.s.
# of SFs per 10 μm
Non-target
α-Actinin KD
E
Non-target
α-Actinin KD
00:00
00:10
00:20
00:30
00:40
F
Non-target
α-Actinin KD
3 μm
5 min
0
5
10 (Min)
G
Myosin IIA-GFP
****
Velocity (nm/sec)
Non-target
α-Actinin KD
H
LifeAct-mCherry
****
Velocity (nm/sec)
Non-target
α-Actinin KD
I
Velocity (nm/sec)
***
**
**
*
NT-DMSO
NT-Blebb
NT-Calyc
KD-DMSO
KD-Blebb
KD-Calyc
J
GFP
ΔABD-GFP
R² = 0.51
R² = -0.02
Velocity (nm/sec)
GFP intensity (a. u.)

Figure 1. SFs are fluidized by inhibiting α-actinin crosslinks

(A) C2C12 cells expressing shRNA against α-actinin (sh α-actinin) or non-targeting shRNA (non-target) were subjected to the western blotting analysis for α-actinin and β-actin.

(B) Representative images of α-actinin KD and non-target (control) C2C12 cells stained for F-actin with phalloidin. White arrowheads indicate "foci" observed in α-actinin KD cells. Scale bars, 20 μm.

(C) Line scan profiles of fluorescence intensities of phalloidin-stained F-actin across SFs in non-target (control) and α-actinin KD cells. Black arrowheads indicate local peak intensities that correspond to SFs. Fluorescence intensities were measured along the yellow lines in inset images of F-actin.

(D) Number densities of SFs in non-target and α-actinin KD cells, which were calculated from line scan profiles (5–12 μm in length each) of fluorescence intensities of phalloidin-stained F-actin. Horizontal bars represent means. n.s., no significant difference; unpaired Student's *t*-test (N = 27–30 places from 9 to 10 cells).

(E) Time-lapse images of LifeAct-mCherry in non-target (control) and α-actinin KD cells. Elapsed time is shown as h:min. Scale bars, 10 μm.

(F) Representative time-lapse fluorescence images and kymographs of myosin IIA-GFP on SFs in α-actinin KD and non-target cells. Scale bars of distance, 3 μm. Scale bars of time in kymographs, 5 min.

(G and H) Velocities of myosin IIA-GFP (G) and LifeAct-mCherry (H) along SFs in non-target and α-actinin KD cells. The velocity was quantified from time-lapse measurements longer than 5 min. Horizontal bars represent means. ****p < 0.0001; Welch's *t*-test (N = 30–35 SFs in 10–12 cells).

(I) Velocities of myosin IIA-GFP along SFs in α-actinin KD and non-target cells treated with DMSO (vehicle), blebbistatin (Blebb, 25 μM), or calyculin A (Calyc, 1 nM) for 5 min. The velocity was quantified from time-lapse measurements longer than 5 min. Horizontal bars represent means. *p < 0.05, **p < 0.01, ***p < 0.001; Tukey's test (N = 20–30 SFs in 6–10 cells).

(J) The velocity of LifeAct-mCherry along SFs was plotted against the fluorescence intensity of GFP for each cell expressing ΔABD-GFP (N = 31 cells) or GFP (N = 22 cells). The velocity value of each dot represents the averaged velocity of LifeAct-mCherry along 3 SFs. Regression lines of linear fitting and Spearman's correlation coefficients (R^2) are also shown. See also Figures S1 and S2.

actin filaments might reduce sliding between actin filaments and, thereby, permit efficient transmission of myosin-generated force to ECM.[39] However, this idea has not been tested experimentally or theoretically, and intracellular machineries responsible for α-actinin-regulated transmission of myosin-generated force to ECM have been unclear.

In the present study, we demonstrate that α-actinin-mediated crosslinks of actin filaments solidify SFs to ensure efficient force transmission along SFs to ECM. Time-lapse imaging and atomic force microscopy (AFM) measurement reveal that inhibition of α-actinin-mediated actin crosslinks reduces elasticity of SFs and fluidizes them. Decreasing the α-actinin crosslink density attenuates traction force exertion to ECM without reducing SF and FA formations and the myosin activity, which suggests that transmission of a contractile force along SFs is diminished. Mathematical model analyses of SF suggest that a reduction in the crosslinker density mobilizes actin filaments along an SF, leading to dissipation of myosin-generated force in an SF through viscous friction of actin filaments against surroundings. At a cellular scale, while cells migrate faster on a softer ECM, fluidization and force dissipation in SFs upon α-actinin depletion attenuate ECM-rigidity-dependent changes in cell migration speed.

RESULTS

SFs fluidize as actin crosslinks are reduced

To examine how actin crosslinkers affect the mechanical properties of SFs, we depleted expression of the major actin-crosslinking protein α-actinin in mouse C2C12 myoblasts using short hairpin RNA (shRNA) targeting all four isoforms of murine α-actinin. C2C12 cells expressed *Actn1* (encoding α-actinin 1) and *Actn4* (encoding α-actinin 4) dominantly and *Actn3* (encoding α-actinin 3) in a lower extent (Figure S1A). Expression of these isoforms was reduced at both mRNA and protein levels by 70%–90% upon pan α-actinin knockdown (KD) (Figures 1A and S1A).

Although α-actinin KD cells sometimes formed SFs thicker than those formed in cells expressing non-targeting shRNA (non-target cells) (Figure 1B), the number density of SFs in individual cells was not altered by α-actinin depletion (Figures 1C and 1D). Furthermore, evaluated by immunostaining the FA marker protein vinculin, the number and size of FAs associated with tips of SFs were not significantly different between α-actinin KD cells and non-target ones (Figures S1B and S1C). However, when we observed dynamics of F-actin and myosin II on SFs in cells expressing myosin IIA-GFP and LifeAct-mCherry, they "flowed" apparently along SFs in α-actinin KD cells without shortening of SFs (Figures 1E and 1F, Videos S1, S2, S3, and S4). Speeds of F-actin and myosin II movements along SFs were approximately 1.7 and 2.2 times faster, respectively, in α-actinin KD cells than those in cells expressing non-targeting shRNA (Figures 1G and 1H). Associated with this, sarcomere organization in SFs was disturbed upon α-actinin depletion; while myosin II and α-actinin were periodically distributed in an alternate manner in non-target cells, myosin II in α-actinin KD cells showed more irregular distribution along SFs (Figures S1D and S1E). We further noticed that α-actinin

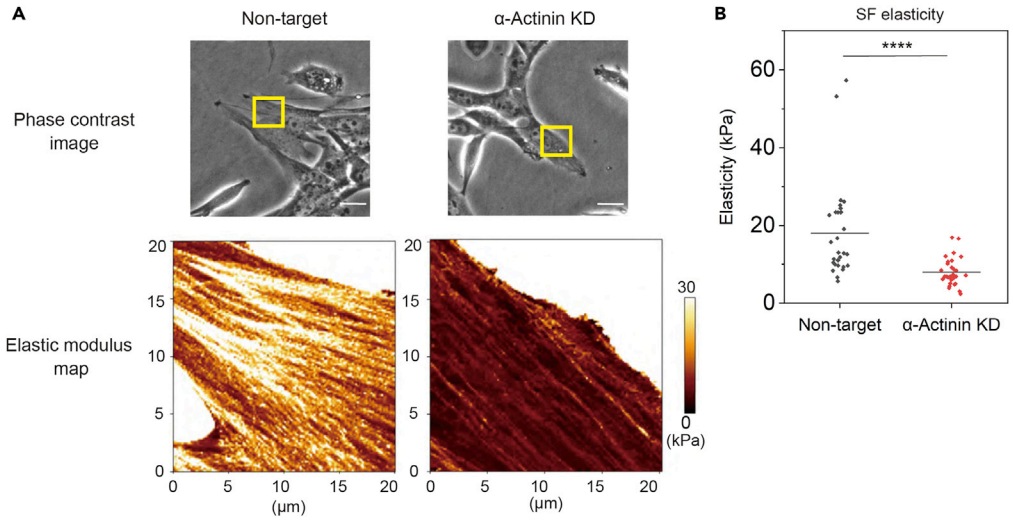

Figure 2. Fluidized SFs are less elastic

(A) Phase-contrast images of non-target and α-actinin KD cells and elastic modulus maps of the boxed regions in the phase-contrast images. The elastic modulus at each point in a 20 × 20-μm area (128 × 128 points) was derived from a force-indentation curve obtained at that point. Scale bars in phase contrast images, 20 μm.

(B) Elastic moduli of SFs in α-actinin KD cells and non-target (control) cells. Horizontal bars represent means.

****$p < 0.0001$; unpaired Student's *t*-test (N = 30 cells). See also Figure S3.

KD cells formed "foci" of actomyosin on SFs, especially at points where multiple SFs were merged (Figures 1B and S2A). These "foci" were observed in 21 of 27 α-actinin KD cells, while only in 7 of 30 non-target cells (Figure S2B). The formation of actomyosin foci was associated with rapid movements of F-actin and myosin II toward the foci-forming sites on SFs (Figure S2C). These results demonstrate that SF components are fluidized upon depletion of α-actinin. When we inhibited the ATPase activity of myosin II with blebbistatin, the speed of the myosin II flow along SFs was significantly lowered both in non-target and α-actinin KD cells (Figure 1I). By contrast, the flow speed became faster by increasing the myosin activity with calyculin A (Figure 1I) that inhibited dephosphorylation of MLC,[40,41] indicating that the flow of SF components along SF was driven by a myosin-generated force.

We further analyzed the effect of α-actinin-mediated actin crosslinking on the mobility of SF components. To this end, we utilized a deleted form of α-actinin 1 lacking the actin-binding domain (ΔABD); ΔABD forms a dimer with endogenous α-actinin 1, thus interfering with α-actinin 1–mediated crosslinks of actin filaments in a dominant-negative fashion,[42] even though it is not clear whether ΔABD forms dimers efficiently with other α-actinin isoforms. When GFP-fused ΔABD (ΔABD-GFP) was expressed, the flow speed of F-actin along SFs was increased with increasing the expression level of ΔABD-GFP ($R^2 = 0.51$), while the expression of GFP alone did not affect the F-actin flow ($R^2 = -0.02$) (Figure 1J). These results show that actin crosslinks by α-actinin are essential for averting fluidization of SFs.

To assess the mechanical status of SFs in a more direct way, we measured their elasticity using AFM. When we constructed elasticity maps of apical surfaces of cells by obtaining a force-indentation curve in each pixel, SFs were characterized as having a linear pattern with high elasticity (Figures 2A and S3).[43–46] The elasticity of individual SFs was significantly lower in α-actinin KD cells than that in non-target cells (Figure 2B), indicating that SFs became less elastic upon depletion of α-actinin.

Our hypothesis that actin crosslinkers affected the fluidity of SFs was further tested by developing a mathematical model of an SF that consisted of dynamically crosslinked actin filaments and myosin II motors (Figure 3A). Based on a simple mathematical insight, effects of repeated associations and dissociations of α-actinin crosslinkers were formulated as a frictional force between actin filaments (see STAR Methods). This friction force was implemented into a practical model of an SF, where a 1-dimensional density field of actin filaments along an SF is defined in a continuum manner, and the density of filaments at both ends was fixed as being adhered to FAs. Here, the force balance along the SF was assumed, i.e., myosin II–induced tension

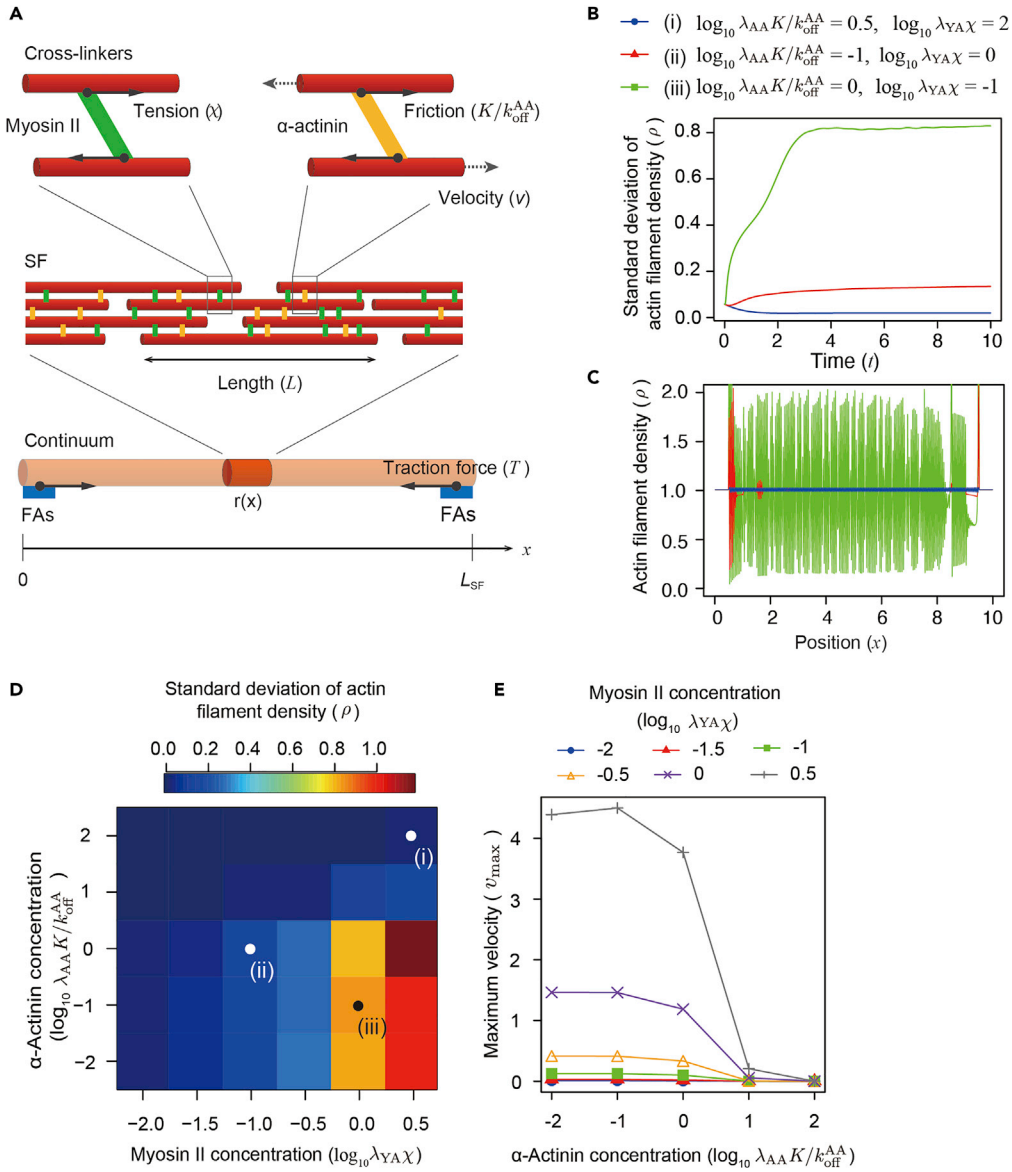

Figure 3. Mathematical modeling analysis of the effect of the crosslinker density on the fluidic property of SFs

(A) A schematic of our mathematical model.

(B) Time evolution of the SD of actin filament density along an SF under different concentrations of α-actinin and myosin II. Blue, red, and green lines represent results obtained under conditions (i), (ii), and (iii), respectively.

(C) Spatial profiles of actin filament density along an SF under different concentrations of α-actinin and myosin II. The profiles were obtained after each simulation reached a steady state. Blue, red, and green lines represent results obtained under conditions (i), (ii), and (iii), respectively.

(D) The SD of actin filament density along an SF is represented by a heatmap in a matrix of different concentrations of α-actinin and myosin II. SD values were calculated after each simulation reached a steady state. (i), (ii), and (iii) in the heatmap correspond to the conditions denoted in (B) and (C).

(E) The averaged maximum velocity of actin filaments along an SF is plotted against the α-actinin concentration in the SF under different myosin II concentrations.

was balanced with inter-filament friction via crosslinkers as well as friction of filaments against the surrounding solvent. Moreover, the mass conservation of filaments was assumed, where filaments flowed along the SF by flux with turnover. The differential equation for the mass conservation was numerically integrated using a Euler scheme to solve the time evolution of the filament density field (see the details in STAR Methods).

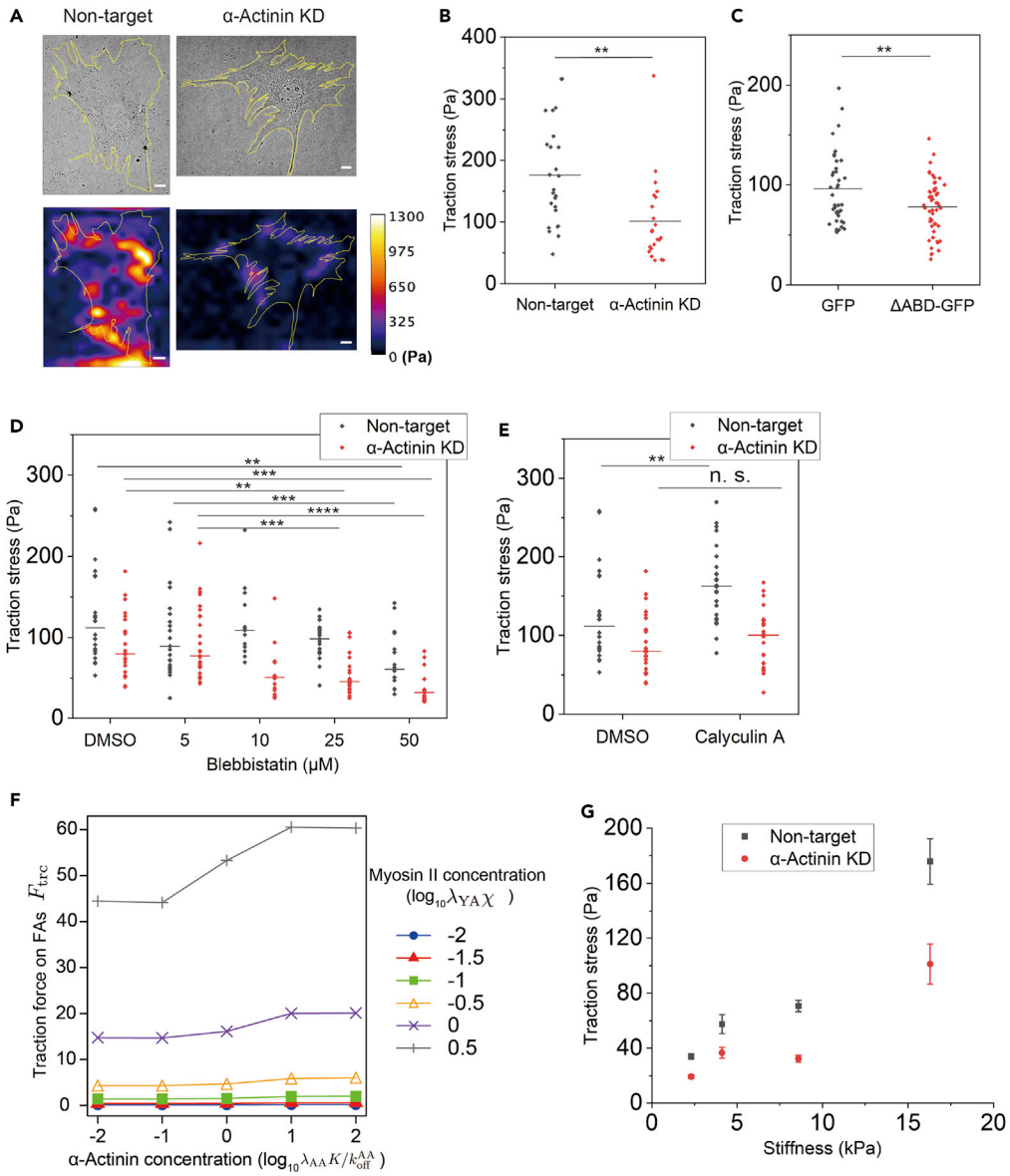

Figure 4. Myosin II–generated force is dissipated in fluidized SFs

(A) Phase-contrast (upper panels) and traction stress (lower panels) images of α-actinin KD and non-target C2C12 cells on fibronectin-coated 16.3-kPa polyacrylamide gel substrates. Yellow lines indicate outlines of cells. The heatmap scale of traction stress is common between non-target and α-actinin KD cells. Scale bars, 10 μm.

(B) Traction stress exerted by non-target (N = 25) and α-actinin KD (N = 22) cells. Horizontal bars represent means. **p < 0.01; unpaired Student's *t*-test.

(C) Traction stress exerted by C2C12 cells expressing GFP (N = 38) or ΔABD-GFP (N = 51). Horizontal bars represent means. **p < 0.01; unpaired Student's *t*-test.

(D) Traction stress exerted by α-actinin KD and non-target cells treated with either blebbistatin (5, 10, 25, or 50 μM) or vehicle (DMSO). Traction stress was measured 10 min after blebbistatin or DMSO was added. Horizontal bars represent means. **p < 0.01, ***p < 0.001; Tukey's test (N = 13–31 cells each).

(E) Traction stress exerted by α-actinin KD and non-target cells treated with either calyculin A (1 nM) or vehicle (DMSO). Traction stress was measured 10 min after calyculin A or DMSO was added. The data for DMSO treatment are the same as those in (D). Horizontal bars represent means. n.s., no significant difference; **p < 0.01; unpaired Student's *t*-test (N = 24–28 cells each).

Figure 4. *Continued*

(F) Traction force acting on FAs at the ends of an SF was simulated in our mathematical model and plotted against the α-actinin concentration in the SF under different myosin II concentrations.

(G) The effect of substrate stiffness on traction stress in α-actinin KD and non-target cells. Cellular traction stresses of cells measured on fibronectin-coated 2.3-kPa, 4.1-kPa, 8.6-kPa, and 16.3-kPa polyacrylamide gel substrates are shown. Each plot indicates mean ± SEM (N = 22–35 cells each). See also Figure S4.

Our model successfully captured the flow of actin filaments in an SF. The resulting filament density field along an SF converged to either a homogeneous or heterogeneous distribution, depending on the concentrations of myosin II and α-actinin (Figures 3B and 3C). The heterogeneity of the filament distribution was found to increase with increasing myosin II concentration and especially drastically with decreasing crosslinker concentration below a certain level (Figure 3D). This feature is consistent with the experimental results that local increases in the actin filament density (F-actin foci) were observed along SFs in α-actinin-depleted cells (Figure S2). Furthermore, the velocity of actin flow increased with increasing myosin II concentration and drastically with decreasing crosslinker concentration (Figure 3E), again suggesting a critical role of actin crosslinkers in determining the fluidic property of SFs.

Fluidized SFs fail to transmit myosin-generated force to FAs

In polymer networks with a viscoelastic nature, force transmitting in the network potentially dissipates through viscous friction.[47] Thus, we reasoned that fluidization of SFs with a reduced crosslinker density might cause dissipation of myosin-generated force transmission in SFs. To test this hypothesis, we measured force transmitting along SFs to FAs by using traction force microscopy.[48–50] Traction stress exerted by α-actinin KD cells (101 ± 14 Pa) was smaller than that exerted by non-target cells (176 ± 17 Pa) (Figures 4A and 4B). Moreover, cells expressing ΔABD-GFP exerted smaller traction stress than cells expressing GFP (Figure 4C). These results demonstrate that depletion of α-actinin crosslinks lowers traction stress exertion to ECM.

A reduction in traction force upon α-actinin depletion would be caused by a reduction in either force generation or force transmission. To discriminate these two potential causes, we examined the effect of α-actinin depletion on myosin force generation by evaluating the phosphorylation status of MLC. When we investigated phosphorylation of MLC at Thr18 and Ser19, an essential step for myosin activation,[51] the relative fluorescence intensity levels of total MLC and MLC di-phosphorylated at Thr18 and Ser19 (PP-MLC) in SFs, which were normalized with the fluorescence intensity of phalloidin staining, were not reduced, but significantly increased, by α-actinin KD, even though mono-phosphorylation of MLC at Ser19 was not affected (Figure S4). These results indicated that the lowered level of traction stress in α-actinin-depleted cells was not attributed to a decrease in the myosin activity.

To further examine the link between the myosin force generation and the traction stress exertion in fluidized SFs, we externally modulated the myosin activity and measured traction stress under the α-actinin-depleted condition. When the myosin II activity was inhibited with blebbistatin, traction stress was decreased in both non-target and α-actinin KD cells, indicating that traction stress was generated by the myosin II activity in both cell types (Figure 4D). On the other hand, even though the calyculin A treatment caused an increase in traction stress in non-target cells, it did not affect traction stress in α-actinin KD cells (Figure 4E), which suggested that elevated myosin II force failed to be transmitted efficiently along fluidized SFs to FAs in α-actinin KD cells.

Properties of force transmission along SFs to FAs were also examined with our mathematical model under different crosslinking conditions. When we measured force exerting at the ends of SFs ("traction force"), the traction force at each myosin II concentration became smaller by lowering the crosslinker concentration (Figure 4F). This demonstrates that even at the same extent of myosin force generation in an SF, the magnitude of force transmitted along an SF to an FA depends on the extent of actin crosslinking. Our model suggested that inefficient force transmission along an SF was caused by slippage of actin filaments due to insufficient α-actinin-mediated crosslinking, where myosin-generated mechanical energy would be dissipated by friction between flowing actin filaments and viscous surroundings (i.e., cytoplasm).

Exertion of myosin II–generated force to ECM is essential for cells to sense the rigidity of ECM, and, conversely, the magnitude of traction force exerted to ECM is reportedly regulated by the ECM

rigidity.[52–54] Given the role of α-actinin in force transmission along SFs to FAs, we wondered whether α-actinin might be involved in rigidity-dependent regulation of cellular traction force. To test this, traction stresses exerted by α-actinin KD cells and non-target ones were measured on the polyacrylamide gel substrates with different rigidities. Traction stress exertion was increased with the substrate rigidity in both cell types, and α-actinin KD cells exerted smaller traction stress than non-target cells throughout the substrate rigidities tested (Figure 4G). Overall, traction stress exertion to ECM was lowered by ~30%–60% upon α-actinin KD (Figure 4G). These results suggest that α-actinin KD cells retain the ability to respond to the ECM rigidity but have a failure in force exertion to ECM.

Actin turnover is accelerated in fluidized SFs

Although depletion of α-actinin induced flows of F-actin and myosin II along SFs, apparent SF structures were maintained in α-actinin KD cells (see Figures 1B–1E). Hence, we next asked how the structural integrity of SFs was maintained under the α-actinin-depleted condition. In the case of filopodia, acceleration of the retrograde flow of F-actin in filopodia is counterbalanced by promotion of actin polymerization to maintain the filopodia length.[55] Reasoned by this, we examined whether the increase in the flow of F-actin along SFs in α-actinin KD cells was associated with enhanced actin polymerization in SFs. To this end, intracellular distribution of the actin polymerization activity was evaluated by monitoring incorporation of fluorescently labeled actin molecules into the actin cytoskeleton in digitonin-permeabilized cells.[56] In non-target cells, fluorescent actin was mainly localized at vinculin-positive FAs (Figures 5A and 5B), sites where actin polymerization is known to be active.[56] However, in α-actinin KD cells, actin incorporation was observed along the entire length of SFs (Figures 5A and 5C), indicating that actin polymerization was promoted throughout SFs. Turnover dynamics of actin molecules in SFs were further examined with fluorescence recovery after photobleaching (FRAP) experiments in cells expressing GFP-tagged actin (Figure 5D, Videos S5 and S6). When we analyzed the mobile fraction and the half recovery time in FRAP of GFP-actin on SFs, the mobile fraction was significantly larger in α-actinin KD cells than that in non-target cells (Figure 5E), while the half recovery time was not altered upon α-actinin depletion (Figure 5F). These results reveal that a larger population of actin molecules in SFs are exchangeable in α-actinin KD cells than those in non-target cells, suggesting that polymerization and depolymerization dynamics of actin on SFs are promoted under α-actinin depletion.

As the LIM domain protein zyxin is reportedly involved in actin polymerization at FAs and on SFs with the aid of Ena/VASP proteins,[56–59] we next examined the effect of α-actinin depletion on intracellular localization of zyxin. Zyxin was preferentially localized at FAs in non-target cells (Figures 6A and 6B). By contrast, it was distributed along the entire length of SFs in α-actinin KD cells (Figures 6A and 6B), which was consistent with the above result that fluorescent actin was incorporated throughout SFs in these cells (Figures 5A and 5C). A deleted form of zyxin that consisted of the LIM domains alone showed a similar localization pattern to that of the full-length zyxin (Figure S5), indicating that the LIM domains of zyxin were sufficient for localizing to α-actinin-depleted SFs.

Previous studies have suggested that LIM domain proteins including zyxin directly bind to tensed actin filaments.[21,60,61] Thus, we examined the role of myosin-generated force in zyxin localization on α-actinin-depleted SFs. Myosin II inhibition with blebbistatin abrogated zyxin localization both at FAs in non-target cells and along SFs in α-actinin KD cells (Figure 6C), which implied that myosin-based tension in actin filaments might be involved in SF localization of zyxin under the α-actinin-depleted condition.

SF fluidization affects cell migration depending on substrate rigidity

We next asked whether α-actinin-mediated modulation of force transmission is involved in cellular signaling and behaviors. The transcriptional coactivator Yes-associated protein (YAP), which plays pivotal roles in fundamental cellular functions including proliferation, differentiation, and survival, is regulated by various mechanical cues such as substrate rigidity and cytoskeletal tension.[62–64] Activated YAP translocates from the cytoplasm to the nucleus to induce transcription of target genes.[63,65] When we examined intracellular distribution of YAP, it localized in the nucleus of non-target cells at a higher extent on stiffer substrates, as expected (Figure S6). The rigidity-dependent nuclear translocation of YAP was not affected by α-actinin depletion (Figure S6), suggesting that α-actinin was not involved in the mechanical regulation of YAP.

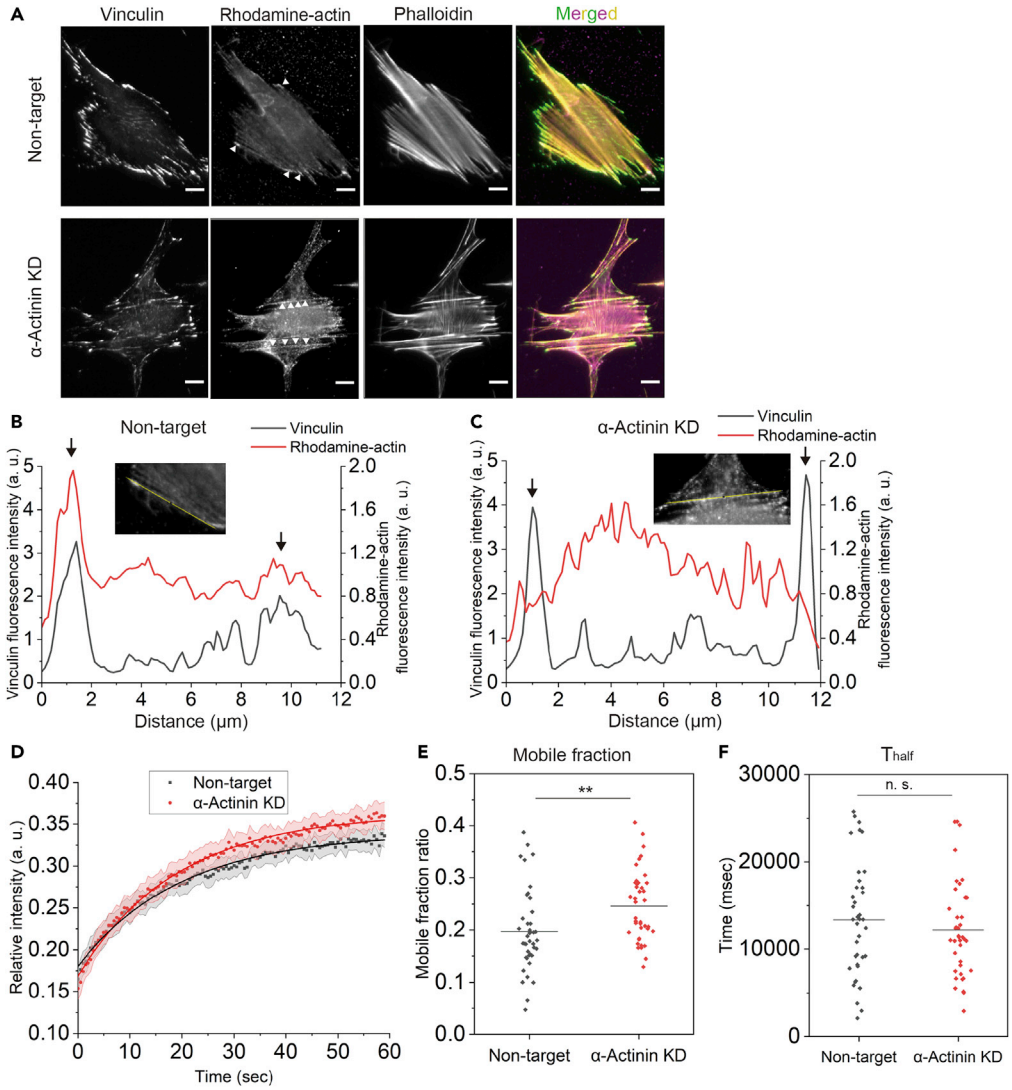

Figure 5. Actin turnover is accelerated in fluidized SFs

(A) Non-target (control) and α-actinin KD C2C12 cells were stained for vinculin and F-actin (with phalloidin) after rhodamine-actin incorporation in the actin polymerization assay. Scale bars, 10 μm.

(B and C) Line profiles of fluorescence intensities of vinculin (black) and rhodamine-actin (red) along SFs in non-target (control) (B) and α-actinin KD (C) cells. The left and right scales are for vinculin and rhodamine-actin intensities, respectively. Fluorescence intensities were measured along SFs indicated by yellow lines in the inset images of rhodamine-actin. Arrows show high fluorescence intensities of vinculin at FAs.

(D) Time-dependent changes of fluorescence intensities of GFP-actin in photobleached regions on SFs in non-target (black) and α-actinin KD (red) cells. Data are shown as mean ± SEM. Regression curves fitted with Equation 2 are also shown. (N = 40 SFs from 15 to 17 cells).

(E and F) Mobile fraction (E) and T_{half} (F) of GFP-actin FRAP on SFs in non-target and α-actinin KD cells. Horizontal bars represent means. n.s., no significant difference; **$p < 0.01$; unpaired Student's *t*-test (N = 38–40 SFs from 15 to 17 cells).

Cell migration is another cellular function that is regulated by intracellular and extracellular mechanical conditions. On one hand, traction force exertion from FAs to ECM drives forward translocation of the cell body.[66] On the other hand, even though assembly/disassembly dynamics of FAs are required for continuous cell migration, the tensile force acting on FAs stabilizes them.[67–69] Thus, it is unclear how the reduced force transmission along fluidized SFs to FAs and ECM affects cell migration. To address this question, we examined the effect of α-actinin depletion on cell migration. Compared with non-target cells, α-actinin KD cells showed smaller cell spread area and a more intricate morphology, diverging from a simple

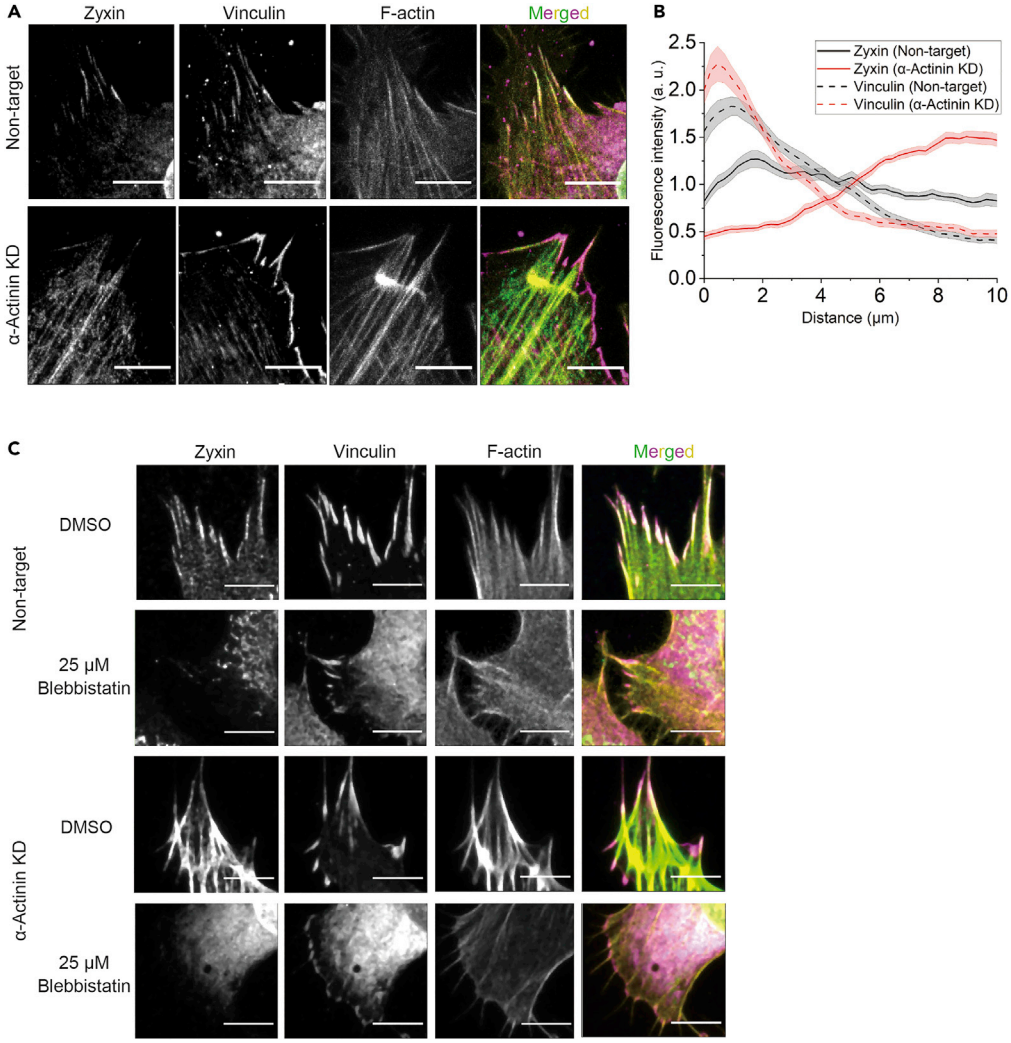

Figure 6. Zyxin localization along fluidized SFs

(A) Non-target (control) and α-actinin KD C2C12 cells stained for zyxin, vinculin, and F-actin (with phalloidin). In merged images, green, magenta, and yellow represent zyxin, vinculin, and F-actin, respectively. Scale bars, 10 μm.

(B) Quantification of fluorescence intensities of zyxin (solid lines) and vinculin (dotted lines) along SFs in non-target (black) and α-actinin KD (red) C2C12 cells. Data are shown as mean ± SEM (N = 39–42 SFs from 9 cells each). The distal edge of each vinculin cluster was defined as a starting point (zero distance), and intensities of zyxin and vinculin were plotted along the connected SF up to 10 μm from the starting point.

(C) Non-target (control) and α-actinin KD cells treated with DMSO (control) or blebbistatin (25 μM) for 30 min were stained for zyxin, vinculin, and F-actin (with phalloidin). In merged images, green, magenta, and yellow represent zyxin, vinculin, and F-actin, respectively. Scale bars, 10 μm. See also Figure S5.

elliptic shape (Figures 7A–7C). When we observed their migration on the glass surface, the migration distance of cells during the observation was significantly larger in α-actinin KD cells than that in non-target cells (Figures 7D and 7E), even though α-actinin depletion did not affect the persistency of cell migration (Figure 7F). Consistently, the velocity of collective cell migration in the wound healing assay was also increased upon α-actinin KD (Figures 7G and 7H). As the traction stress magnitude was dependent on the substrate rigidity (see Figure 4G), we next investigated cell migration on the substrates with different rigidities. The velocity of individual cell migration was higher on the soft substrate (2.3 kPa) than that on the stiff substrate (i.e., glass) in both non-target and α-actinin KD cells (Figures 7D and 7E). Interestingly, depletion of α-actinin expression significantly decreased the velocity of cell migration on the soft substrate (Figures 7D and 7E), which was in marked contrast to the above observation that the cell migration velocity

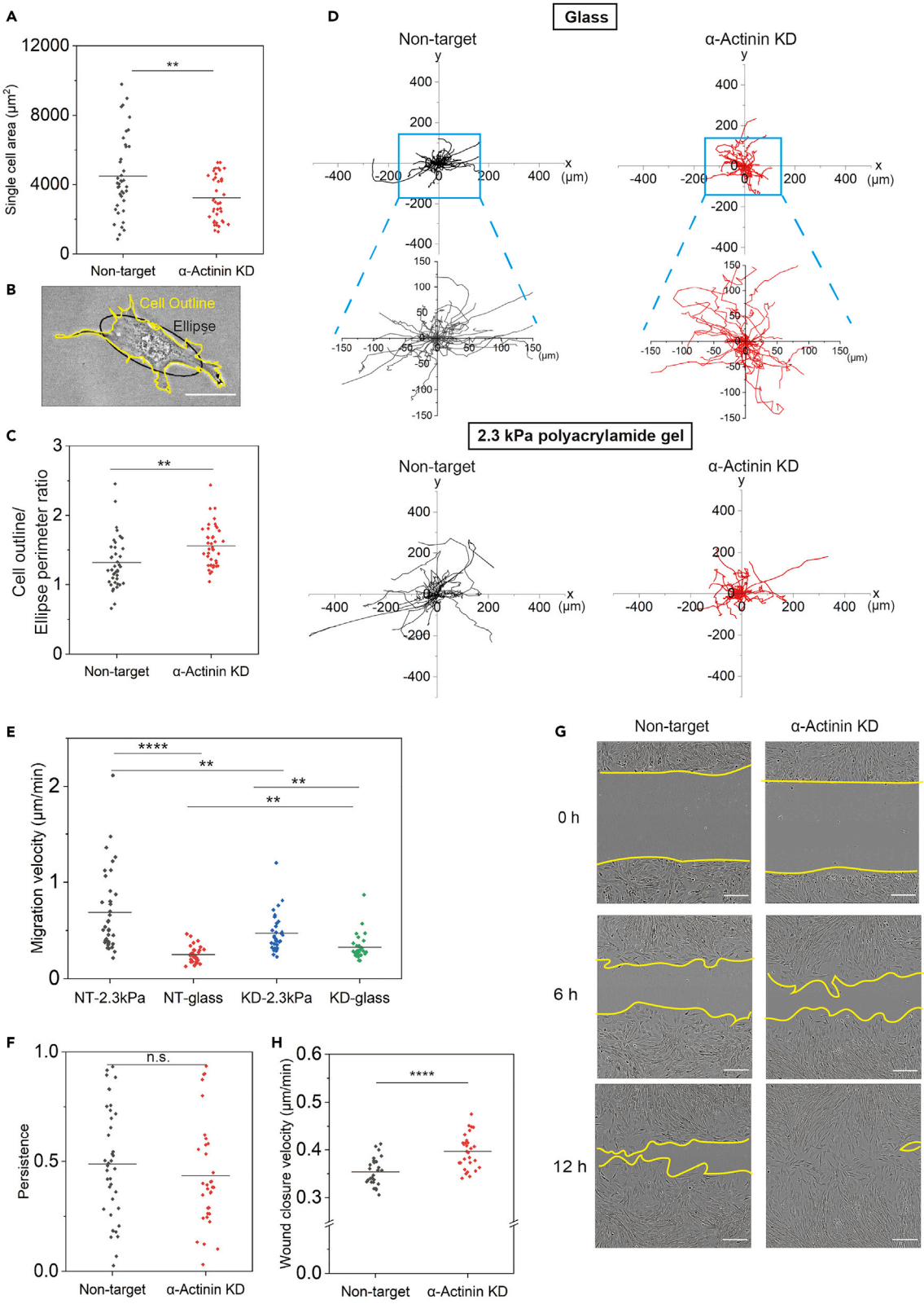
A
Single cell area (μm²)
12000
8000
4000
0
**
Non-target
α-Actinin KD
B
Cell Outline
Ellipse
C
Cell outline/
Ellipse perimeter ratio
3
2
1
0
**
Non-target
α-Actinin KD
D
Glass
Non-target
α-Actinin KD
y
x
(μm)
2.3 kPa polyacrylamide gel
Non-target
α-Actinin KD
E
Migration velocity (μm/min)
2
1
0
****
**
**
**
NT-2.3kPa
NT-glass
KD-2.3kPa
KD-glass
F
Persistence
1.0
0.5
0.0
n.s.
Non-target
α-Actinin KD
H
Wound closure velocity (μm/min)
0.6
0.5
0.4
0.3
0.0
****
Non-target
α-Actinin KD
G
Non-target
α-Actinin KD
0 h
6 h
12 h

Figure 7. The role of α-actinin in rigidity-dependent regulation of cell migration speed

(A) Area of individual α-actinin KD and non-target (control) C2C12 cells. Horizontal bars represent means. **p < 0.01; unpaired *t*-test (N = 39–40 cells).

(B) An example of the cell outline (yellow) and ellipse fitting (black) of a cell. Scale bars, 50 μm.

(C) The cell outline/ellipse perimeter ratio of α-actinin KD and non-target (control) C2C12 cells. Horizontal bars represent means. **p < 0.01; unpaired *t*-test (N = 39–40 cells).

(D) Rose plots depicting migration trajectories of individual non-target and α-actinin KD cells for 240 min on fibronectin-coated glass (upper panels) or 2.3-kPa polyacrylamide gel (lower panels) substrates (N = 31–34 cells). Magnified views of the cell trajectories on glass are also shown.

(E) The migration velocity of non-target and α-actinin KD cells on fibronectin-coated glass and 2.3-kPa polyacrylamide gel substrates. Horizontal bars represent means. **p < 0.01, ****p < 0.0001; Welch's *t*-test (N = 31–38 cells).

(F) Persistence of migration of non-target (N = 39) and α-actinin KD (N = 33) cells on fibronectin-coated glass. Horizontal bars represent means. n.s., not significant; unpaired Student's *t*-test.

(G) Time-lapse images of non-target (upper panels) and α-actinin KD (lower panels) cells in the wound healing assay. Yellow lines indicate the wound edges. Scale bars, 200 μm.

(H) Velocity of wound closure of non-target and α-actinin KD cells. Horizontal bars represent means. ****p < 0.0001; unpaired Student's *t*-test; (N = 30 samples). See also Figure S6.

was increased by α-actinin depletion on the glass substrate (Figures 7D and 7E). Consequently, the difference in cell migration speed on substrates with different rigidities became less apparent upon α-actinin KD (Figures 7D and 7E), which suggested involvement of α-actinin in sensing and/or responding to the substrate rigidity during cell migration.

DISCUSSION

With experimental and computational analyses, we demonstrate that α-actinin-mediated actin crosslinking solidifies SFs by diminishing slippage of F-actin and myosin II in SFs, which ensures transmission of myosin II–generated force along SFs and exertion of traction force to ECM. Under the condition where α-actinin crosslinks are inhibited, SFs are fluidized with flows of F-actin and myosin II, resulting in viscous dissipation of transmitting force in SFs. Hence, exogenous elevation of the myosin II activity in α-actinin-depleted cells fails to increase traction force exertion to ECM.

Previous studies have shown that α-actinin 4 (ACTN4) K255E mutation, which increases the binding affinity of α-actinin 4 for F-actin, makes the actin filament network more elastic and solid-like both *in vitro* and in cells.[39,70–72] Moreover, the expression of K255E-mutated α-actinin 4 reportedly increases traction stress exertion to ECM.[39] These results suggest involvement of α-actinin-actin binding in modulating mechanics and force transmission in the actin cytoskeletal systems, which is consistent with our results. In contrast to our study, other studies have shown an inhibitory role of α-actinin in cell traction force exertion.[42,44,49] One possible basis underlying this discrepancy may be the difference in stages of cell morphogenesis. In our present study, we have analyzed traction force exertion in cells showing the polarized morphology with developed SFs, in which myosin II–generated contractile force in SFs is transmitted to ECM as traction force.[13,19] By contrast, Roca-Cusachs et al.[42] and Oakes et al.[48] analyzed cells in the initial spreading stage and showed that simultaneous depletion of α-actinin 1 and α-actinin 4 led to increased traction force exertion in these cells. In spreading cells, myosin II–driven retrograde flow of the actin network in extending lamella provides a major source of traction force; force is transmitted from the retrograding actin cytoskeleton to ECM-bound integrins via the "molecular clutch" mechanism.[73–76] Thus, α-actinin depletion in spreading cells may fluidize the actin cytoskeleton and facilitate its retrograde flow, which potentially results in elevation of traction force exertion in these cells. This scenario is distinct from our finding of α-actinin-mediated force transmission along solidified SFs to ECM and needs to be tested in future studies.

Under the α-actinin depletion, myosin II–generated force induced flows of F-actin and myosin II along SFs. Even though these flows frequently caused local accumulations of F-actin and myosin II in SFs, SFs were rarely severed or collapsed. Thus, the cable integrity of α-actinin-depleted SFs is maintained under the dynamic steady state. Indeed, we showed that α-actinin KD promoted actin polymerization in SFs, which might reinforce SFs. Furthermore, we found that the LIM domain protein zyxin, which facilitates actin polymerization with the aid of Ena/VASP proteins,[56,57,59] translocated from FAs to the entire length of SFs upon α-actinin depletion. Recent studies have shown that LIM domain proteins including zyxin directly bind to tensed actin filaments, which is involved in the repair of thinned, stretched sites in SFs.[21,59–61] Zyxin localization throughout SFs in α-actinin KD cells may also be mediated by the tensile status of actin filaments, as this localization depends on the myosin II activity (Figure 6C). When the density of α-actinin-mediated

crosslinks of actin filaments is low, only a small population of actin filaments in an SF would be involved in transmitting myosin force at each time point, and these filaments would sustain a larger tensile force than those in SFs with the high α-actinin density. These highly tensed actin filaments may provide zyxin-binding sites in α-actinin-depleted SFs.

Recently, it has been reported that zyxin contributes to elastic behaviors of SFs.[21] On the other hand, we found in the present study that inhibition of α-actinin-mediated crosslinks of actin filaments caused significant fluidization of SFs even in the presence of zyxin association with SFs. Our results suggest that α-actinin plays a more dominant role in determining the mechanical property of SFs than zyxin.

We found that the cell migration speed was affected by α-actinin expression. Interestingly, this effect was dependent on the stiffness of extracellular substrates; while α-actinin depletion increased the cell migration speed on the stiff (glass) substrate, the speed on the soft (2.3 kPa) substrate was lowered by depleting α-actinin. The mechanism underlying the differential effects of substrate stiffness on α-actinin-mediated regulation of cell migration is currently unclear. However, the balance between cellular traction force and stability of FAs may be involved. In a migrating cell, traction force exertion at FAs to the extracellular substrate is responsible for dragging the cell body forward. At the same time, for continuous cell migration, the assembly/disassembly cycle of FAs is required; when FAs, as the feet of a cell, are too stable and not disassembled, the cell is stuck to the extracellular substrate and cannot move further.[77] Notably, the stability of FAs is potentially regulated by the traction force magnitude and the substrate stiffness; cells exert a larger traction force on stiffer substrates, and a larger traction force at FAs makes FAs more stable.[52,78] Therefore, on the hard surface of glass, FAs in control cells may be highly stabilized by a large traction force, which would result in the low migration speed in these cells. However, a reduction in traction force by α-actinin depletion may promote FA turnover and thereby accelerate cell migration on the stiff substrate. By contrast, on the soft substrate, on which the intrinsic level of cellular traction force is low, knocking down α-actinin may make the traction force too small to efficiently drive cell migration.

α-Actinin-mediated sensing of the substrate rigidity[79] may also be involved in the rigidity-dependent regulation of cell migration. As a minimal machinery for rigidity sensing, a single-sarcomere-like complex called the CU has been found in spreading cells.[79–81] CUs regulate protrusion-retraction cycles of cellular leading edges depending on the substrate rigidity.[79] Similar to SFs, CUs are composed of actin and myosin II filaments, tropomyosin and α-actinin.[79–81] Thus, it is conceivable that α-actinin averts slippage of actin and myosin II filaments in both CUs of single-sarcomere units and SFs of multiple sarcomere units in series. Stabilization of these contractile machineries by α-actinin may underlie the rigidity-dependent regulation of leading edge dynamics in migrating cells.

Given that force communication between cells and extracellular surroundings modulates various cellular behaviors including migration, morphogenesis, survival, proliferation, and differentiation,[82,83] it is plausible that a defect in α-actinin-mediated transmission of actomyosin force influences a wide range of tissue and organ functions. Indeed, several mutations in α-actinin 4, which increase the binding affinity of α-actinin 4 to F-actin, are known to cause the kidney disease, familial focal segmental glomerulosclerosis.[84] These α-actinin 4 mutations make the actin cytoskeleton stiffened and tensed, leading to the actin cytoskeleton breakage and cell detachment in podocytes that are repeatedly stretched due to expansion-retraction cycles of glomerular capillaries.[85,86] As another example, α-actinin-mediated force transmission may be involved in muscle differentiation and regeneration. Our finding that actin crosslinking by α-actinin is required for sarcomere-like organization in myoblasts is consistent with the essential role of α-actinin in Z-disk formation during myogenesis.[87] Furthermore, α-actinin may contribute also to myoblast fusion into myotubes. Upon contact with myoblasts, fusion pores are formed in contacting plasma membranes. In the region surrounding the fusion pore, F-actin, myosin II, and α-actinin are accumulated.[88,89] While actomyosin contraction in this region expands the fusion pore to complete cell-cell fusion,[90,91] α-actinin may promote this process by ensuring force transmission from the actomyosin complex to the fusion pore. Furthermore, when muscle is regenerated after injury, the myogenic progenitor cells, satellite cells, migrate to the damaged site in muscle for restoration,[92] where α-actinin may be involved in the regulation of satellite cell migration. Further studies addressing whether and how α-actinin-mediated force transmission contributes to our health and disease may lead to the development of novel strategies for clinical treatments targeting actin cytoskeleton mechanics.

Limitations of the study

In this study, we find that α-actinin-mediated actin crosslinking solidifies SFs by averting slippage between actin filaments in SFs, which ensures transmission of myosin II–generated forces along SFs and exertion of traction force to ECM. However, some major questions remain to be solved. First, do actin crosslinkers other than α-actinin, such as filamin and fascin, also contribute to mechanical properties of SFs? These crosslinkers may contribute to the structural integrity of SFs under the α-actinin-depleted condition. Second, the detailed mechanisms of how α-actinin-mediated crosslinks regulate cell migration and rigidity sensing need to be revealed from molecular and biophysical points of view. Furthermore, it is of great interest how α-actinin-modulated SF mechanics relate to physiological or pathological functions of tissues.

STAR★METHODS

Detailed methods are provided in the online version of this paper and include the following:

- KEY RESOURCES TABLE
- RESOURCE AVAILABILITY
  - Lead contact
  - Materials availability
  - Data and code availability
- EXPERIMENTAL MODEL AND SUBJECT DETAILS
  - Cell culture
- METHOD DETAILS
  - Plasmids, transfection, and retroviral infection
  - Quantitative RT-PCR (qRT-PCR)
  - Antibody
  - Time-lapse imaging
  - Polyacrylamide gel substrate
  - Traction force microscopy
  - Immunofluorescence
  - Western blotting
  - Measurement of Feret diameters of FAs
  - Quantification of cell area and cell shape
  - Sigle cell migration assay
  - Wound healing assay
  - Actin polymerization assay
  - FRAP analysis
  - Atomic force microscopy (AFM)
  - Modeling and numerical simulation
- QUANTIFICATION AND STATISTICAL ANALYSIS

SUPPLEMENTAL INFORMATION

Supplemental information can be found online at https://doi.org/10.1016/j.isci.2023.106090.

ACKNOWLEDGMENTS

We thank Keiko Kawauchi, Robert Adelstein, Pere Roca-Cusachs, and Michael Sheetz for providing cells and plasmid constructs, Nagoya University Center for Gene Research for sequencing plasmid DNA, and Division for Medical Research Engineering for allowing to use microscopes and a gene electroporator. This study was supported by the grant for collaborative research between Nagoya University and R-Pharm (2614Dj-02b to M.S.), JSPS KAKENHI (20K12596 to H.H., 21H05127 to H.H., 22H05170 to S.O., 21H03804 to K.N., 22K19890 to K.N., 19H01147 to M.K., 22KK0145 to M.K., and 21K18326 to S.K.), JST CREST (JPMJCR1921 to S.O.), AMED (21bm0704065h0002 to S.O.), and Nagoya University Kyosaidan. This work was the result of using research equipment shared in the MEXT project for promoting public utilization of an advanced research infrastructure (program for supporting construction of core facilities; grant number JPMXS044110XX).

AUTHOR CONTRIBUTIONS

Conceptualization, H.K., S.O., and H.H.; Investigation, H.K., S.O., K.N., H.M., and H.H.; Mathematical Modeling, S.O.; AFM Measurement, K.N.; Results Discussion, H.K., S.O., K.N., S.K., M.K., M.S., T.M., and H.H.; Writing the Manuscript, H.K., S.O., K.N., M.S., and H.H.

DECLARATION OF INTERESTS

The authors declare no competing interests.

Received: June 6, 2022
Revised: January 13, 2023
Accepted: January 25, 2023
Published: February 1, 2023

REFERENCES

1. Vicente-Manzanares, M., Ma, X., Adelstein, R.S., and Horwitz, A.R. (2009). Non-muscle myosin II takes centre stage in cell adhesion and migration. Nat. Rev. Mol. Cell Biol. *10*, 778–790. https://doi.org/10.1038/nrm2786.

2. Bruyère, C., Versaevel, M., Mohammed, D., Alaimo, L., Luciano, M., Vercruysse, E., and Gabriele, S. (2019). Actomyosin contractility scales with myoblast elongation and enhances differentiation through YAP nuclear export. Sci. Rep. *9*, 15565–15614. https://doi.org/10.1038/s41598-019-52129-1.

3. Engler, A.J., Sen, S., Sweeney, H.L., and Discher, D.E. (2006). Matrix elasticity directs stem cell lineage specification. Cell *126*, 677–689. https://doi.org/10.1016/j.cell.2006.06.044.

4. Salbreux, G., Charras, G., and Paluch, E. (2012). Actin cortex mechanics and cellular morphogenesis. Trends Cell Biol. *22*, 536–545. https://doi.org/10.1016/J.TCB.2012.07.001.

5. Mukhina, S., Wang, Y.L., and Murata-Hori, M. (2007). α-Actinin is required for tightly regulated remodeling of the actin cortical network during cytokinesis. Dev. Cell *13*, 554–565. https://doi.org/10.1016/J.DEVCEL.2007.08.003.

6. Green, R.A., Paluch, E., and Oegema, K. (2012). Cytokinesis in animal cells. Annu. Rev. Cell Dev. Biol. *28*, 29–58. https://doi.org/10.1146/ANNUREV-CELLBIO-101011-155718.

7. Goldman, Y.E. (1987). Kinetics of the actomyosin ATPase in muscle fibers. Annu. Rev. Physiol. *49*, 637–654. https://doi.org/10.1146/annurev.ph.49.030187.003225.

8. Ridley, A.J., and Hall, A. (1992). The small GTP-binding protein rho regulates the assembly of focal adhesions and actin stress fibers in response to growth factors. Cell *70*, 389–399. https://doi.org/10.1016/0092-8674(92)90163-7.

9. Burridge, K., and Guilluy, C. (2016). Focal adhesions, stress fibers and mechanical tension. Exp. Cell Res. *343*, 14–20. https://doi.org/10.1016/J.YEXCR.2015.10.029.

10. Harris, A.K., Wild, P., and Stopak, D. (1980). Silicone rubber substrata: a new wrinkle in the study of cell locomotion. Science *208*, 177–179. https://doi.org/10.1126/science.6987736.

11. Chrzanowska-Wodnicka, M., and Burridge, K. (1996). Rho-stimulated contractility drives the formation of stress fibers and focal adhesions. J. Cell Biol. *133*, 1403–1415. https://doi.org/10.1083/jcb.133.6.1403.

12. Balaban, N.Q., Schwarz, U.S., Riveline, D., Goichberg, P., Tzur, G., Sabanay, I., Mahalu, D., Safran, S., Bershadsky, A., Addadi, L., and Geiger, B. (2001). Force and focal adhesion assembly: a close relationship studied using elastic micropatterned substrates. Nat. Cell Biol. *3*, 466–472. https://doi.org/10.1038/35074532.

13. Livne, A., and Geiger, B. (2016). The inner workings of stress fibers – from contractile machinery to focal adhesions and back. J. Cell Sci. *129*, 1293–1304. https://doi.org/10.1242/JCS.180927.

14. Chapin, L.M., Blankman, E., Smith, M.A., Shiu, Y.T., and Beckerle, M.C. (2012). Lateral communication between stress fiber sarcomeres facilitates a local remodeling response. Biophys. J. *103*, 2082–2092. https://doi.org/10.1016/J.BPJ.2012.09.038.

15. Smith, M.A., Hoffman, L.M., and Beckerle, M.C. (2014). LIM proteins in actin cytoskeleton mechanoresponse. Trends Cell Biol. *24*, 575–583. https://doi.org/10.1016/J.TCB.2014.04.009.

16. Zaidel-Bar, R., Zhenhuan, G., and Luxenburg, C. (2015). The contractome–a systems view of actomyosin contractility in non-muscle cells. J. Cell Sci. *128*, 2209–2217. https://doi.org/10.1242/JCS.170068.

17. Kiss, A., Erdődi, F., and Lontay, B. (2019). Myosin phosphatase: unexpected functions of a long-known enzyme. Biochim. Biophys. Acta Mol. Cell Res. *1866*, 2–15. https://doi.org/10.1016/J.BBAMCR.2018.07.023.

18. Álvarez-Santos, M.D., Álvarez-González, M., Estrada-Soto, S., and Bazán-Perkins, B. (2020). Regulation of myosin light-chain phosphatase activity to generate airway smooth muscle hypercontractility. Front. Physiol. *11*, 701. https://doi.org/10.3389/FPHYS.2020.00701.

19. Kumar, S., Maxwell, I.Z., Heisterkamp, A., Polte, T.R., Lele, T.P., Salanga, M., Mazur, E., and Ingber, D.E. (2006). Viscoelastic retraction of single living stress fibers and its impact on cell shape, cytoskeletal organization, and extracellular matrix mechanics. Biophys. J. *90*, 3762–3773. https://doi.org/10.1529/biophysj.105.071506.

20. Tanner, K., Boudreau, A., Bissell, M.J., and Kumar, S. (2010). Dissecting regional variations in stress fiber mechanics in living cells with laser nanosurgery. Biophys. J. *99*, 2775–2783. https://doi.org/10.1016/J.BPJ.2010.08.071.

21. Oakes, P.W., Wagner, E., Brand, C.A., Probst, D., Linke, M., Schwarz, U.S., Glotzer, M., and Gardel, M.L. (2017). Optogenetic control of RhoA reveals zyxin-mediated elasticity of stress fibres. Nat. Commun. *8*, 15817–15912. https://doi.org/10.1038/ncomms15817.

22. Kemp, J.P., and Brieher, W.M. (2018). The actin filament bundling protein α-actinin-4 actually suppresses actin stress fibers by permitting actin turnover. J. Biol. Chem. *293*, 14520–14533. https://doi.org/10.1074/JBC.RA118.004345.

23. Cramer, L.P., Siebert, M., and Mitchison, T.J. (1997). Identification of novel graded polarity actin filament bundles in locomoting heart fibroblasts: implications for the generation of motile force. J. Cell Biol. *136*, 1287–1305. https://doi.org/10.1083/JCB.136.6.1287.

24. Pellegrin, S., and Mellor, H. (2007). Actin stress fibres. J. Cell Sci. *120*, 3491–3499. https://doi.org/10.1242/JCS.018473.

25. Lieleg, O., Schmoller, K.M., Claessens, M.M.A.E., and Bausch, A.R. (2009). Cytoskeletal polymer networks: viscoelastic properties are determined by the microscopic interaction potential of cross-links. Biophys. J. *96*, 4725–4732. https://doi.org/10.1016/J.BPJ.2009.03.038.

26. Schmoller, K.M., Lieleg, O., and Bausch, A.R. (2009). Structural and viscoelastic properties

of actin/filamin networks: cross-linked versus bundled networks. Biophys. J. *97*, 83–89. https://doi.org/10.1016/J.BPJ.2009.04.040.

27. Gardel, M.L., Kasza, K.E., Brangwynne, C.P., Liu, J., and Weitz, D.A. (2008). Mechanical response of cytoskeletal networks. Methods Cell Biol. *89*, 487–519. https://doi.org/10.1016/S0091-679X(08)00619-5.

28. Kasza, K.E., Rowat, A.C., Liu, J., Angelini, T.E., Brangwynne, C.P., Koenderink, G.H., and Weitz, D.A. (2007). The cell as a material. Curr. Opin. Cell Biol. *19*, 101–107. https://doi.org/10.1016/J.CEB.2006.12.002.

29. Weihs, D., Mason, T.G., and Teitell, M.A. (2006). Bio-microrheology: a frontier in microrheology. Biophys. J. *91*, 4296–4305. https://doi.org/10.1529/BIOPHYSJ.106.081109.

30. Lazarides, E., and Burridge, K. (1975). α-Actinin: immunofluorescent localization of a muscle structural protein in nonmuscle cells. Cell *6*, 289–298. https://doi.org/10.1016/0092-8674(75)90180-4.

31. Sjöblom, B., Salmazo, A., and Djinović-Carugo, K. (2008). α-Actinin structure and regulation. Cell. Mol. Life Sci. *65*, 2688–2701. https://doi.org/10.1007/S00018-008-8080-8.

32. Foley, K.S., and Young, P.W. (2014). The non-muscle functions of actinins: an update. Biochem. J. *459*, 1–13. https://doi.org/10.1042/BJ20131511.

33. Le, S., Hu, X., Yao, M., Chen, H., Yu, M., Xu, X., Nakazawa, N., Margadant, F.M., Sheetz, M.P., and Yan, J. (2017). Mechanotransmission and mechanosensing of human alpha-actinin 1. Cell Rep. *21*, 2714–2723. https://doi.org/10.1016/j.celrep.2017.11.040.

34. Ylänne, J., Scheffzek, K., Young, P., and Saraste, M. (2001). Crystal structure of the α-actinin rod reveals an extensive torsional twist. Structure *9*, 597–604. https://doi.org/10.1016/S0969-2126(01)00619-0.

35. Pavalko, F.M., and Burridge, K. (1991). Disruption of the actin cytoskeleton after microinjection of proteolytic fragments of alpha-actinin. J. Cell Biol. *114*, 481–491. https://doi.org/10.1083/JCB.114.3.481.

36. Feng, Y., Ngu, H., Alford, S.K., Ward, M., Yin, F., and Longmore, G.D. (2013). α-Actinin1 and 4 tyrosine phosphorylation is critical for stress fiber establishment, maintenance and focal adhesion maturation. Exp. Cell Res. *319*, 1124–1135. https://doi.org/10.1016/j.yexcr.2013.02.009.

37. Choi, C.K., Vicente-Manzanares, M., Zareno, J., Whitmore, L.A., Mogilner, A., and Horwitz, A.R. (2008). Actin and α-actinin orchestrate the assembly and maturation of nascent adhesions in a myosin II motor-independent manner. Nat. Cell Biol. *10*, 1039–1050. https://doi.org/10.1038/NCB1763.

38. Wachsstock, D.H., Schwarz, W.H., and Pollard, T.D. (1994). Cross-linker dynamics determine the mechanical properties of actin gels. Biophys. J. *66*, 801–809. https://doi.org/10.1016/S0006-3495(94)80856-2.

39. Ehrlicher, A.J., Krishnan, R., Guo, M., Bidan, C.M., Weitz, D.A., and Pollak, M.R. (2015). Alpha-actinin binding kinetics modulate cellular dynamics and force generation. Proc. Natl. Acad. Sci. USA *112*, 6619–6624. https://doi.org/10.1073/PNAS.1505652112.

40. Watanabe, T., Hosoya, H., and Yonemura, S. (2007). Regulation of myosin II dynamics by phosphorylation and dephosphorylation of its light chain in epithelial cells. Mol. Biol. Cell *18*, 605–616. https://doi.org/10.1091/MBC.E06-07-0590.

41. Suzuki, A., and Itoh, T. (1993). Effects of calyculin A on tension and myosin phosphorylation in skinned smooth muscle of the rabbit mesenteric artery. Br. J. Pharmacol. *109*, 703–712. https://doi.org/10.1111/j.1476-5381.1993.tb13631.x.

42. Roca-Cusachs, P., del Rio, A., Puklin-Faucher, E., Gauthier, N.C., Biais, N., and Sheetz, M.P. (2013). Integrin-dependent force transmission to the extracellular matrix by α-actinin triggers adhesion maturation. Proc. Natl. Acad. Sci. USA *110*, E1361–E1370. https://doi.org/10.1073/pnas.1220723110.

43. Nagayama, K., Ohata, S., Obata, S., and Sato, A. (2020). Macroscopic and microscopic analysis of the mechanical properties and adhesion force of cells using a single cell tensile test and atomic force microscopy: remarkable differences in cell types. J. Mech. Behav. Biomed. Mater. *110*, 103935. https://doi.org/10.1016/J.JMBBM.2020.103935.

44. Doss, B.L., Pan, M., Gupta, M., Grenci, G., Mège, R.M., Lim, C.T., Sheetz, M.P., Voituriez, R., and Ladoux, B. (2020). Cell response to substrate rigidity is regulated by active and passive cytoskeletal stress. Proc. Natl. Acad. Sci. USA *117*, 12817–12825. https://doi.org/10.1073/PNAS.1917555117.

45. Gavara, N., and Chadwick, R.S. (2016). Relationship between cell stiffness and stress fiber amount, assessed by simultaneous atomic force microscopy and live-cell fluorescence imaging. Biomech. Model. Mechanobiol. *15*, 511–523. https://doi.org/10.1007/S10237-015-0706-9.

46. Haga, H., Sasaki, S., Kawabata, K., Ito, E., Ushiki, T., and Sambongi, T. (2000). Elasticity mapping of living fibroblasts by AFM and immunofluorescence observation of the cytoskeleton. Ultramicroscopy *82*, 253–258. https://doi.org/10.1016/S0304-3991(99)00157-6.

47. Sabass, B., and Schwarz, U.S. (2010). Modeling cytoskeletal flow over adhesion sites: competition between stochastic bonddynamics and intracellular relaxation. J. Phys. Condens. Matter *22*, 194112. https://doi.org/10.1088/0953-8984/22/19/194112.

48. Oakes, P.W., Beckham, Y., Stricker, J., and Gardel, M.L. (2012). Tension is required but not sufficient for focal adhesion maturation without a stress fiber template. J. Cell Biol. *196*, 363–374. https://doi.org/10.1083/jcb.201107042.

49. Gardel, M.L., Sabass, B., Ji, L., Danuser, G., Schwarz, U.S., and Waterman, C.M. (2008). Traction stress in focal adhesions correlates biphasically with actin retrograde flow speed. J. Cell Biol. *183*, 999–1005. https://doi.org/10.1083/jcb.200810060.

50. Dembo, M., Oliver, T., Ishihara, A., and Jacobson, K. (1996). Imaging the traction stresses exerted by locomoting cells with the elastic substratum method. Biophys. J. *70*, 2008–2022. https://doi.org/10.1016/S0006-3495(96)79767-9.

51. Sakurada, K., Seto, M., and Sasaki, Y. (1998). Dynamics of myosin light chain phosphorylation at Ser19 and Thr18/Ser19 in smooth muscle cells in culture. Am. J. Physiol. *274*, C1563–C1572. https://doi.org/10.1152/ajpcell.1998.274.6.C1563.

52. Trichet, L., Le Digabel, J., Hawkins, R.J., Vedula, S.R.K., Gupta, M., Ribrault, C., Hersen, P., Voituriez, R., and Ladoux, B. (2012). Evidence of a large-scale mechanosensing mechanism for cellular adaptation to substrate stiffness. Proc. Natl. Acad. Sci. USA *109*, 6933–6938. https://doi.org/10.1073/PNAS.1117810109.

53. Yip, A.K., Iwasaki, K., Ursekar, C., Machiyama, H., Saxena, M., Chen, H., Harada, I., Chiam, K.H., and Sawada, Y. (2013). Cellular response to substrate rigidity is governed by either stress or strain. Biophys. J. *104*, 19–29. https://doi.org/10.1016/j.bpj.2012.11.3805.

54. Hirata, H., Ku, W.C., Yip, A.K., Ursekar, C.P., Kawauchi, K., Roy, A., Guo, A.K., Vedula, S.R.K., Harada, I., Chiam, K.H., et al. (2016). MEKK1-dependent phosphorylation of calponin-3 tunes cell contractility. J. Cell Sci. *129*, 3574–3582. https://doi.org/10.1242/jcs.189415.

55. Anderson, T.W., Vaughan, A.N., and Cramer, L.P. (2008). Retrograde flow and myosin II activity within the leading cell edge deliver F-actin to the lamella to seed the formation of graded polarity actomyosin II filament bundles in migrating fibroblasts. Mol. Biol. Cell *19*, 5006–5018. https://doi.org/10.1091/mbc.e08-01-0034.

56. Hirata, H., Tatsumi, H., and Sokabe, M. (2008). Mechanical forces facilitate actin polymerization at focal adhesions in a zyxin-dependent manner. J. Cell Sci. *121*, 2795–2804. https://doi.org/10.1242/JCS.030320.

57. Nix, D.A., Fradelizi, J., Bockholt, S., Menichi, B., Louvard, D., Friederich, E., and Beckerle, M.C. (2001). Targeting of zyxin to sites of actin membrane interaction and to the nucleus. J. Biol. Chem. *276*, 34759–34767. https://doi.org/10.1074/JBC.M102820200.

58. Yoshigi, M., Hoffman, L.M., Jensen, C.C., Yost, H.J., and Beckerle, M.C. (2005). Mechanical force mobilizes zyxin from focal adhesions to actin filaments and regulates cytoskeletal reinforcement. J. Cell Biol. *171*,

209–215. https://doi.org/10.1083/JCB.200505018.

59. Smith, M.A., Blankman, E., Gardel, M.L., Luettjohann, L., Waterman, C.M., and Beckerle, M.C. (2010). A zyxin-mediated mechanism for actin stress fiber maintenance and repair. Dev. Cell *19*, 365–376. https://doi.org/10.1016/j.devcel.2010.08.008.

60. Sun, X., Phua, D.Y.Z., Axiotakis, L., Smith, M.A., Blankman, E., Gong, R., Cail, R.C., Espinosa de Los Reyes, S., Beckerle, M.C., Waterman, C.M., and Alushin, G.M. (2020). Mechanosensing through direct binding of tensed F-actin by LIM domains. Dev. Cell *55*, 468–482.e7. https://doi.org/10.1016/j.devcel.2020.09.022.

61. Winkelman, J.D., Anderson, C.A., Suarez, C., Kovar, D.R., and Gardel, M.L. (2020). Evolutionarily diverse LIM domain-containing proteins bind stressed actin filaments through a conserved mechanism. Proc. Natl. Acad. Sci. USA *117*, 25532–25542. https://doi.org/10.1073/PNAS.2004656117.

62. Dupont, S., Morsut, L., Aragona, M., Enzo, E., Giulitti, S., Cordenonsi, M., Zanconato, F., Le Digabel, J., Forcato, M., Bicciato, S., et al. (2011). Role of YAP/TAZ in mechanotransduction. Nature *474*, 179–183. https://doi.org/10.1038/nature10137.

63. Dobrokhotov, O., Samsonov, M., Sokabe, M., and Hirata, H. (2018). Mechanoregulation and pathology of YAP/TAZ via Hippo and non-Hippo mechanisms. Clin. Transl. Med. *7*, 23. https://doi.org/10.1186/S40169-018-0202-9.

64. Panciera, T., Azzolin, L., Cordenonsi, M., and Piccolo, S. (2017). Mechanobiology of YAP and TAZ in physiology and disease. Nat. Rev. Mol. Cell Biol. *18*, 758–770. https://doi.org/10.1038/NRM.2017.87.

65. Dupont, S. (2016). Role of YAP/TAZ in cell-matrix adhesion-mediated signalling and mechanotransduction. Exp. Cell Res. *343*, 42–53. https://doi.org/10.1016/J.YEXCR.2015.10.034.

66. Fournier, M.F., Sauser, R., Ambrosi, D., Meister, J.J., and Verkhovsky, A.B. (2010). Force transmission in migrating cells. J. Cell Biol. *188*, 287–297. https://doi.org/10.1083/JCB.200906139.

67. Metzner, C., Raupach, C., Zitterbart, D.P., and Fabry, B. (2007). Simple model of cytoskeletal fluctuations. Phys. Rev. E - Stat. Nonlinear Soft Matter Phys. *76*, 021925. https://doi.org/10.1103/PhysRevE.76.021925.

68. Raupach, C., Zitterbart, D.P., Mierke, C.T., Metzner, C., Müller, F.A., and Fabry, B. (2007). Stress fluctuations and motion of cytoskeletal-bound markers. Phys. Rev. E - Stat. Nonlinear Soft Matter Phys. *76*, 011918. https://doi.org/10.1103/PhysRevE.76.011918.

69. Lange, J.R., and Fabry, B. (2013). Cell and tissue mechanics in cell migration. Exp. Cell Res. *319*, 2418–2423. https://doi.org/10.1016/J.YEXCR.2013.04.023.

70. Yao, N.Y., Broedersz, C.P., Depken, M., Becker, D.J., Pollak, M.R., MacKintosh, F.C., and Weitz, D.A. (2013). Stress-enhanced gelation: a dynamic nonlinearity of elasticity. Phys. Rev. Lett. *110*, 018103. https://doi.org/10.1103/PHYSREVLETT.110.018103.

71. Yao, N.Y., Becker, D.J., Broedersz, C.P., Depken, M., MacKintosh, F.C., Pollak, M.R., and Weitz, D.A. (2011). Nonlinear viscoelasticity of actin transiently cross-linked with mutant α-actinin-4. J. Mol. Biol. *411*, 1062–1071. https://doi.org/10.1016/J.JMB.2011.06.049.

72. Broedersz, C.P., Depken, M., Yao, N.Y., Pollak, M.R., Weitz, D.A., and MacKintosh, F.C. (2010). Cross-link-governed dynamics of biopolymer networks. Phys. Rev. Lett. *105*, 238101. https://doi.org/10.1103/PHYSREVLETT.105.238101.

73. Elosegui-Artola, A., Oria, R., Chen, Y., Kosmalska, A., Pérez-González, C., Castro, N., Zhu, C., Trepat, X., and Roca-Cusachs, P. (2016). Mechanical regulation of a molecular clutch defines force transmission and transduction in response to matrix rigidity. Nat. Cell Biol. *18*, 540–548. https://doi.org/10.1038/ncb3336.

74. Case, L.B., and Waterman, C.M. (2015). Integration of actin dynamics and cell adhesion by a three-dimensional, mechanosensitive molecular clutch. Nat. Cell Biol. *17*, 955–963. https://doi.org/10.1038/NCB3191.

75. Hu, K., Ji, L., Applegate, K.T., Danuser, G., and Waterman-Storer, C.M. (2007). Differential transmission of actin motion within focal adhesions. Science *315*, 111–115. https://doi.org/10.1126/SCIENCE.1135085.

76. Brown, C.M., Hebert, B., Kolin, D.L., Zareno, J., Whitmore, L., Horwitz, A.R., and Wiseman, P.W. (2006). Probing the integrin-actin linkage using high-resolution protein velocity mapping. J. Cell Sci. *119*, 5204–5214. https://doi.org/10.1242/JCS.03321.

77. Ridley, A.J., Schwartz, M.A., Burridge, K., Firtel, R.A., Ginsberg, M.H., Borisy, G., Parsons, J.T., and Horwitz, A.R. (2003). Cell migration: integrating signals from front to back. Science *302*, 1704–1709. https://doi.org/10.1126/SCIENCE.1092053.

78. Zhou, D.W., Lee, T.T., Weng, S., Fu, J., and García, A.J. (2017). Effects of substrate stiffness and actomyosin contractility on coupling between force transmission and vinculin-paxillin recruitment at single focal adhesions. Mol. Biol. Cell *28*, 1901–1911. https://doi.org/10.1091/MBC.E17-02-0116.

79. Meacci, G., Wolfenson, H., Liu, S., Stachowiak, M.R., Iskratsch, T., Mathur, A., Ghassemi, S., Gauthier, N., Tabdanov, E., Lohner, J., et al. (2016). α-Actinin links extracellular matrix rigidity-sensing contractile units with periodic cell-edge retractions. Mol. Biol. Cell *27*, 3471–3479. https://doi.org/10.1091/MBC.E16-02-0107.

80. Ghassemi, S., Meacci, G., Liu, S., Gondarenko, A.A., Mathur, A., Roca-Cusachs, P., Sheetz, M.P., and Hone, J. (2012). Cells test substrate rigidity by local contractions on submicrometer pillars. Proc. Natl. Acad. Sci. USA *109*, 5328–5333. https://doi.org/10.1073/PNAS.1119886109.

81. Wolfenson, H., Meacci, G., Liu, S., Stachowiak, M.R., Iskratsch, T., Ghassemi, S., Roca-Cusachs, P., O'Shaughnessy, B., Hone, J., and Sheetz, M.P. (2016). Tropomyosin controls sarcomere-like contractions for rigidity sensing and suppressing growth on soft matrices. Nat. Cell Biol. *18*, 33–42. https://doi.org/10.1038/ncb3277.

82. Jaalouk, D.E., and Lammerding, J. (2009). Mechanotransduction gone awry. Nat. Rev. Mol. Cell Biol. *10*, 63–73. https://doi.org/10.1038/nrm2597.

83. Vining, K.H., and Mooney, D.J. (2017). Mechanical forces direct stem cell behaviour in development and regeneration. Nat. Rev. Mol. Cell Biol. *18*, 728–742. https://doi.org/10.1038/nrm.2017.108.

84. Kaplan, J.M., Kim, S.H., North, K.N., Rennke, H., Correia, L.A., Tong, H.Q., Mathis, B.J., Rodríguez-Pérez, J.C., Allen, P.G., Beggs, A.H., and Pollak, M.R. (2000). Mutations in ACTN4, encoding α-actinin-4, cause familial focal segmental glomerulosclerosis. Nat. Genet. *24*, 251–256. https://doi.org/10.1038/73456.

85. Feng, D., Notbohm, J., Benjamin, A., He, S., Wang, M., Ang, L.H., Bantawa, M., Bouzid, M., Del Gado, E., Krishnan, R., and Pollak, M.R. (2018). Disease-causing mutation in α-actinin-4 promotes podocyte detachment through maladaptation to periodic stretch. Proc. Natl. Acad. Sci. USA *115*, 1517–1522. https://doi.org/10.1073/PNAS.1717870115.

86. Kriz, W., and Lemley, K.V. (2015). A potential role for mechanical forces in the detachment of podocytes and the progression of CKD. J. Am. Soc. Nephrol. *26*, 258–269. https://doi.org/10.1681/ASN.2014030278.

87. Salucci, S., Baldassarri, V., Falcieri, E., and Burattini, S. (2015). α-Actinin involvement in Z-disk assembly during skeletal muscle C2C12 cells in vitro differentiation. Micron *68*, 47–53. https://doi.org/10.1016/J.MICRON.2014.08.010.

88. Duan, R., Kim, J.H., Shilagardi, K., Schiffhauer, E.S., Lee, D.M., Son, S., Li, S., Thomas, C., Luo, T., Fletcher, D.A., et al. (2018). Spectrin is a mechanoresponsive protein shaping fusogenic synapse architecture during myoblast fusion. Nat. Cell Biol. *20*, 688–698. https://doi.org/10.1038/s41556-018-0106-3.

89. Kim, J.H., Ren, Y., Ng, W.P., Li, S., Son, S., Kee, Y.S., Zhang, S., Zhang, G., Fletcher, D.A., Robinson, D.N., and Chen, E.H. (2015). Mechanical tension drives cell membrane fusion. Dev. Cell *32*, 561–573. https://doi.org/10.1016/J.DEVCEL.2015.01.005.

90. Cong, J., Fang, B., Wang, Q., Su, Y., Gu, T., and Luo, T. (2019). The mechanobiology of actin cytoskeletal proteins during cell–cell fusion. J. R. Soc. Interface *16*, 20190022. https://doi.org/10.1098/RSIF.2019.0022.

91. Duan, R., and Gallagher, P.J. (2009). Dependence of myoblast fusion on a cortical actin wall and nonmuscle myosin IIA. Dev. Biol. *325*, 374–385. https://doi.org/10.1016/j.ydbio.2008.10.035.

92. Thomas, K., Engler, A.J., and Meyer, G.A. (2015). Extracellular matrix regulation in the muscle satellite cell niche. Connect. Tissue Res. *56*, 1–8. https://doi.org/10.3109/03008207.2014.947369.

93. Kawauchi, K., Tan, W.W., Araki, K., Abu Bakar, F.B., Kim, M., Fujita, H., Hirata, H., and Sawada, Y. (2012). p130Cas-dependent actin remodelling regulates myogenic differentiation. Biochem. J. *445*, 323–332. https://doi.org/10.1042/BJ20112169.

94. Wei, Q., and Adelstein, R.S. (2000). Conditional expression of a truncated fragment of nonmuscle myosin II-A alters cell shape but not cytokinesis in HeLa cells. Mol. Biol. Cell *11*, 3617–3627. https://doi.org/10.1091/MBC.11.10.3617.

95. Guo, A.K., Hou, Y.Y., Hirata, H., Yamauchi, S., Yip, A.K., Chiam, K.H., Tanaka, N., Sawada, Y., and Kawauchi, K. (2014). Loss of p53 enhances NF-κB-Dependent lamellipodia formation. J. Cell. Physiol. *229*, 696–704. https://doi.org/10.1002/JCP.24505.

96. Ebata, T., Mitsui, Y., Sugimoto, W., Maeda, M., Araki, K., Machiyama, H., Harada, I., Sawada, Y., Fujita, H., Hirata, H., and Kawauchi, K. (2017). Substrate stiffness influences doxorubicin-induced p53 activation via ROCK2 expression. BioMed Res. Int. *2017*, 5158961. https://doi.org/10.1155/2017/5158961.

97. Syed, S., Schober, J., Blanco, A., and Zustiak, S.P. (2017). Morphological adaptations in breast cancer cells as a function of prolonged passaging on compliant substrates. PLoS One *12*, e0187853. https://doi.org/10.1371/JOURNAL.PONE.0187853.

98. Plotnikov, S.V., Sabass, B., Schwarz, U.S., and Waterman, C.M. (2014). High-Resolution traction force microscopy. Methods Cell Biol. *123*, 367–394. https://doi.org/10.1016/B978-0-12-420138-5.00020-3.

99. Plotnikov, S.V., Pasapera, A.M., Sabass, B., and Waterman, C.M. (2012). Force fluctuations within focal adhesions mediate ECM-rigidity sensing to guide directed cell migration. Cell *151*, 1513–1527. https://doi.org/10.1016/j.cell.2012.11.034.

100. Sabass, B., Gardel, M.L., Waterman, C.M., and Schwarz, U.S. (2008). High resolution traction force microscopy based on experimental and computational advances. Biophys. J. *94*, 207–220. https://doi.org/10.1529/biophysj.107.113670.

101. Tseng, Q., Duchemin-Pelletier, E., Deshiere, A., Balland, M., Guillou, H., Filhol, O., and Théry, M. (2012). Spatial organization of the extracellular matrix regulates cell-cell junction positioning. Proc. Natl. Acad. Sci. USA *109*, 1506–1511. https://doi.org/10.1073/pnas.1106377109.

102. Conrad, P.A., Nederlof, M.A., Herman, I.M., and Taylor, D.L. (1989). Correlated distribution of actin, myosin, and microtubules at the leading edge of migrating Swiss 3T3 fibroblasts. Cell Motil Cytoskeleton *14*, 527–543. https://doi.org/10.1002/CM.970140410.

103. Sprague, B.L., and McNally, J.G. (2005). FRAP analysis of binding: proper and fitting. Trends Cell Biol. *15*, 84–91. https://doi.org/10.1016/J.TCB.2004.12.001.

104. Tawada, K., and Sekimoto, K. (1991). Protein friction exerted by motor enzymes through a weak-binding interaction. J. Theor. Biol. *150*, 193–200. https://doi.org/10.1016/S0022-5193(05)80331-5.

105. Hannezo, E., Dong, B., Recho, P., Joanny, J.F., and Hayashi, S. (2015). Cortical instability drives periodic supracellular actin pattern formation in epithelial tubes. Proc. Natl. Acad. Sci. USA *112*, 8620–8625. https://doi.org/10.1073/PNAS.1504762112.

106. Feramisco, J.R., and Blose, S.H. (1980). Distribution of flourescently labeled α-actinin in living and fixed fibroblasts. J. Cell Biol. *86*, 608–615. https://doi.org/10.1083/JCB.86.2.608.94.

STAR★METHODS

KEY RESOURCES TABLE

REAGENT or RESOURCE	SOURCE	IDENTIFIER
Antibodies		
Mouse, monoclonal, anti α-actinin	Merck-Millipore	Cat# AT6/172
Mouse, monoclonal, anti β-actin	Sigma-Aldrich	Cat# A5441
Rabbit, polyclonal, anti-myosin light chain 2	Cell Signaling Technology	Cat# 3672; RRID:AB_10692513
Rabbit, polyclonal, anti-phospho (Ser19)-myosin light chain 2	Cell Signaling Technology	Cat# 3671; RRID:AB_330248
Rabbit, polyclonal, anti-di-phospho (Thr18/Ser19)-myosin light chain 2	Cell Signaling Technology	Cat# 3674; RRID:AB_2147464
Mouse, monoclonal, anti-vinculin	Sigma-Aldrich	Cat# V9131; RRID:AB_477629
Mouse, monoclonal, anti-YAP	Santa-Cruz Biotechnology	Cat# sc-101199; RRID:AB_1131430
Rabbit, monoclonal, anti-zyxin	Sigma-Aldrich	Cat# 2F17
Goat, Alexa Fluor™ 488 conjugated, polyclonal, anti-mouse IgG (H+L)	Thermo Fisher Scientific	Cat# A11001; RRID:AB_2534069
Goat, Alexa Fluor™ 546, conjugated, polyclonal, anti-rabbit IgG (H+L)	Thermo Fisher Scientific	Cat# A11035; RRID:AB_143051
Goat, HRP conjugated, polyclonal, anti-mouse IgG	Cell Signaling Technology	Cat# 7076; RRID:AB_330924
Goat, HRP conjugated, polyclonal, anti-rabbit IgG	Cell Signaling Technology	Cat# 7074; RRID:AB_2099233
Chemicals, peptides, and recombinant proteins		
Actin protein (rhodamine)	Cytoskeleton	Cat# APHR-A
Carboxylated silicon–rhodamine (SiR)-actin	Cytoskeleton	Cat# CY-SC001
4-12% Bis-Tris gel 12 well	Thermo Fisher Scientific	Cat# NP0322
Lipofectamine 3000	Thermo Fisher Scientific	Cat# L3000008
3-aminopropyltrimethoxysilane	Wako Chemical	Cat# 323-74352
GeneJuice	Merck-Millipore	Cat# 70967
Hygromycin B	Fujifilm Wako	Cat# 085-06153
Ammonium Persulfate	Fujifilm Wako	Cat# 016-20501
N,N,N′,N′-tetramethylethylenediamine	AppliChem	Cat# A1148
sulfo-SANPAH	Thermo Fisher Scientific	Cat# 22589
Fluoresbrite YG Microspheres - 0.20 µm	Polyscience	Cat# 17151-10
Fluoresbrite YO Carboxylate Microspheres - 0.20 µm	Polyscience	Cat# 19391-10
Calyculin A	Sigma Aldrich	Cat# C5552
(-)-Blebbistatin	Toronto Research Chemicals	Cat# B592500
Para-amino-blebbistatin	Cayman Chemical	Cat# 22699
SuperSignal™ West Femto Maximum Sensitivity Substrate	Thermo Fisher Scientific	Cat# 34094
Digitonin	Fujifilm Wako	Cat# 044-02121
Protease Inhibitor Cocktail	Sigma Aldrich	Cat# P8340
Fibronectin human plasma	Sigma Aldrich	Cat# F2006
4x lithium dodecyl sulfate buffer	Thermo Fisher Scientific	Cat# NP0007
Experimental models: Cell lines		
C2C12	Kawauchi et al.[93]	A gift from Keiko Kawauchi
HEK293T	Kawauchi et al.[93]	A gift from Keiko Kawauchi

(*Continued on next page*)

Continued

REAGENT or RESOURCE	SOURCE	IDENTIFIER
Oligonucleotides		
shRNA for α-actinin knockdown 5′-GTGCCAGCTGGAGATCAAC-3′	ThermoFisher Scientific	Custom synthesis
shRNA for α-actinin knockdown 5′-ATAGTCACAGACATTAGGT-3′	ThermoFisher Scientific	Custom synthesis
Actn1 (encoding α-actinin 1) forward primer 5′-CCACTTTGACCGGGATCACT-3′	Eurofin Genomics	Custom synthesis
Actn1 (encoding α-actinin 1) reverse primer 5′-CGGTTGGGGTCTACAATGCT-3′	Eurofin Genomics	Custom synthesis
Actn2 (encoding α-actinin 2) forward primer 5′-TTGGATGCTGAAGGCCGAGA-3′	Eurofin Genomics	Custom synthesis
Actn2 (encoding α-actinin 2) reverse primer 5′-GTTCTCCAGCCAGGGGATTG-3′	Eurofin Genomics	Custom synthesis
Actn3 (encoding α-actinin 3) forward primer 5′-GACTGCTGCCAACAGGATCT-3′	Eurofin Genomics	Custom synthesis
Actn3 (encoding α-actinin 3) reverse primer 5′-CGGTTCTCTAGCCATGGGAC-3′	Eurofin Genomics	Custom synthesis
Actn4 (encoding α-actinin 4) forward primer 5′-ACAAGCTGCGGAAGGATGAT-3′	Eurofin Genomics	Custom synthesis
Actn4 (encoding α-actinin 4) reverse primer 5′-ATTATGGCCTTCTCGTCGGG-3′	Eurofin Genomics	Custom synthesis
Gapdh forward primer 5′-AGGTCGGTGTGAACGGATTTG-3′	Eurofin Genomics	Custom synthesis
Gapdh reverse primer 5′-TGTAGACCATGTAGTTGAGGTCA-3′	Eurofin Genomics	Custom synthesis
Recombinant DNA		
GFP-tagged human zyxin	Hirata et al.[56]	N/A
GFP-tagged fragment of zyxin encoding the LIM region	Hirata et al.[56]	N/A
pAmpho	Ebata et al.[96]	A gift from Keiko Kawauchi
pSUPER.retro.hygro	Guo et al.[95]	A gift from Keiko Kawauchi
mCherry-tagged LifeAct	This paper	N/A
GFP-tagged actin	This paper	N/A
GFP-tagged, deleted form of α-actinin lacking the actin binding domain	Roca-Cusachs et al.[42]	Addgene Plasmid #66935
GFP-tagged human myosin IIA heavy chain	Wei and Adelstein[94]	Addgene Plasmid #11347
Software and algorithms		
ImageJ (Fiji) (Ver. 1.52)	NIH, ImageJ	https://imagej.net/software/fiji/
Origin Pro	OriginLab	https://www.originlab.com/
NIS-Elements AR	Nikon	https://www.nikon.com/products/industrial-metrology/lineup/microscope/img_soft/nis-elements/
Custom C++ program to simulate stress fiber dynamics	This paper	https://doi.org/10.5281/zenodo.7509409

RESOURCE AVAILABILITY

Lead contact

Further information and requests for resources and reagents should be directed to and will be fulfilled by the Lead Contact, Hiroaki Hirata (hirata@neptune.kanazawa-it.ac.jp).

Materials availability

Plasmid constructs generated in this study are listed in the key resources table and available from the lead contact on request.

Data and code availability

- All data reported in this paper will be shared by the lead contact upon request.
- The source code for SF model simulation has been posted in the GitHub site and is publicly available as of the date of publication. DOI is listed in the key resources table.
- Any additional information required to reanalyze the data reported in this paper is available from the lead contact upon request.

EXPERIMENTAL MODEL AND SUBJECT DETAILS

Cell culture

C2C12[93] cells and HEK293T[93] cells were maintained in Dulbecco's modified Eagle's medium (DMEM) supplemented with 10% fetal bovine serum, 50 units/mL penicillin and 50 μg/mL streptomycin (all from Gibco) at 37°C in 5% CO_2. For experiments, cells were grown for 16-24 hours on the substrates indicated.

METHOD DETAILS

Plasmids, transfection, and retroviral infection

GFP-tagged human full-length zyxin (Zyxin-GFP) and a fragment of zyxin encoding the LIM region (ZyxLIM-GFP) were described previously.[56] The mCherry-tagged LifeAct and GFP-tagged actin constructs were generated by subcloning annealed oligonucleotides encoding the LifeAct sequence (3′-GGTGTCGCA GATTTGATCAAGAAATTCGAAAGCATCTCAAAGGAAGAA-5′) or PCR-amplified DNA encoding the actin sequence into pcDNA3 vector containing the mCherry or GFP sequence, respectively. GFP-tagged human myosin IIA heavy chain (CMV-GFP-NMHC II-A) was gifted from Robert Adelstein (Addgene plasmid # 11347; http://n2t.net/addgene:11347; RRID:Addgene_11347).[94] A GFP-tagged, deleted form of α-actinin lacking the actin binding domain (ΔABD-GFP) was gifted from Pere Roca-Cusachs and Michael Sheetz (Addgene plasmid # 66935; http://n2t.net/addgene:66935; RRID: Addgene_66935).[42] These plasmids were transfected into cells using Lipofectamine 3000 reagent (Thermo Fisher Scientific), according to the manufacturer's protocol. Cells were analyzed 24-48 hours after transfection.

In traction force microscopy (TFM) experiments, the GFP or ΔABD-GFP plasmid was introduced into cells by electroporation using NEPA21 electroporator (Nepagene). 2.0-10.0 x 10^5 cells were suspended in 100 μL serum-free DMEM with 5 μg plasmid. Electroporation was carried out with two poring pulses (150 V, 5 ms) and three transfer pulses (20 V, 50 ms).

Short hairpin RNA (shRNA)-mediated stable knockdown of α-actinin was conducted using the retroviral system. The sequence 5′-GTGCCAGCTGGAGATCAAC-3′ targeting all four isoforms of murine α-actinin was inserted into the pSUPER.retro.hygro retroviral vector (a gift from Keiko Kawauchi).[95] For control, the non-targeting sequence 5′-ATAGTCACAGACATTAGGT-3′ was introduced. The shRNA sequence-containing vector was co-transfected with the pAmpho vector (a gift from Keiko Kawauchi)[96] into HEK293T cells using the GeneJuice transfection reagent (Merck Millipore). Supernatants containing viral particles were harvested 24-48 hours after the transfection, filtered through 0.45-μm PVDF membrane, and added to the C2C12 cell culture with 8 μg/mL polybrene. Infected cells were selected with 1000 μg/mL hygromycin for 48-96 hours.

Quantitative RT-PCR (qRT-PCR)

Total RNA was isolated from C2C12 cells with TRIzol (Thermo Fischer Scientific) according to the manufacturer's protocol. RNA was then subjected to cDNA synthesis using High Capacity cDNA Reverse Transcription Kit (Thermo Fischer Scientific). cDNA was mixed with FastStart Universal SYBR Green Master (Roche) and primer oligo DNA of mouse GAPDH or an α-actinin isoform (see key resources table for primer sequences). PCR was performed with Thermal Cycler Dice Real Time System (Takara) according to the manufacturer's protocol.

Antibody

The primary and secondary antibodies used in this study are shown in the key resources table.

Time-lapse imaging

Cells expressing fluorescently tagged proteins were seeded in DMEM onto 35-mm glass bottom dish (Iwaki) or μ-dish 35 mm Quad (Ibidi) that was pre-coated with 50 μg/mL fibronectin. Cells were observed 3-8 hours after seeding. In the experiments of pharmacological treatments, observation was carried out 5 min after the drug application. The cells were observed using the inverted confocal microscope (A1Rsi, Nikon) equipped with an oil-immersion objective lens (NA 1.49, 60x, Apo-TIRF, Nikon or NA 1.45, 100x, Plan Apo, Nikon) and a heat chamber (TOKAI-HIT) under the 37°C and 5% CO_2 humidified atmosphere.

Acquired images were analyzed using Fiji or NIS-Elements AR (Nikon) software. The average flow speed of myosin IIA-GFP or LifeAct-mCherry in each SF was calculated based on the slope in the kymograph depicted using Multi Kymograph tool in Fiji. This measurement was carried out for three SFs in each cell.

Polyacrylamide gel substrate

Composition and stiffness of polyacrylamide (PAAm) gel substrates used in this study (Table S1) were described previously.[97,98] Using the stock solutions of acrylamide (Wako Chemical) and bisacrylamide (Wako Chemical) mixtures, gel preparation solutions containing yellow-green or red fluorescent beads with 0.2 μm diameter (Polysciences; for gel substrates used in traction force microscopy), ammonium persulfate (Wako Chemical) and N,N,N′,N′-tetramethylethylenediamine (AppliChem) were prepared immediately before use. We placed 18 μL of the gel preparation solution onto a glass-bottom dish (35 mm diameter) that was silanized with 1% 3-aminopropyltrimethoxysilane (Wako Chemical) for 15 min at room temperature, washed with methanol and air dried, and then the solution was covered with a bare glass coverslip (22 mm diameter). After polymerization of acrylamide for 30 min, the top coverslip was carefully removed and the gel was fully hydrated in HEPES buffer (100 mM HEPES, pH 7.5 (Wako Chemical)). Whilst previous studies[98–100] used acrylamide solution at the volume/area ratio of 0.023-0.039 $\mu L/mm^2$, the ratio in our study was 0.047 $\mu L/mm^2$. Given that thickness of the gel prepared from 0.039 $\mu L/mm^2$ solution was ~50 μm,[52] thickness of our gel was estimated as about 60 μm. This thickness is about 20-60 times larger than the traction-force-induced deformation of the gel (ca. 1-3 μm).

Fibronectin was immobilized on the PAAm gel surface using sulfo-SANPAH (Thermo Fisher Scientific). One millimolar sulfo-SANPAH in HEPES buffer was placed onto the PAAm gel surface and exposed to ultraviolet (UV) light for 10 min. The darkened sulfo-SANPAH solution was removed, and gels were rinsed three times with HEPES buffer, incubated with 100 mg/mL fibronectin (Sigma) at 37°C for 1 hour, and then washed three times with HEPES buffer. After equilibration with DMEM overnight at 4°C, the gels were used for experiments.

Traction force microscopy

Cells were seeded and grown on fibronectin-conjugated, fluorescent bead-embedded PAAm gel substrates for 16-24 hr. Cells and fluorescent beads were observed with an inverted epifluorescence microscope (BZ-710, Keyence) equipped with a 60x objective lens (NA 1.20, Plan Fluor, Nikon). Bright field images of cells as well as fluorescence images of embedded beads were acquired before and after detaching the cells from the gel substrates by trypsinization. When indicated, cells were treated with para-amino-blebbistatin (Cayman Chemical) (5, 10, 25 or 50 μM), calyculin A (1 nM) or vehicle (DMSO) for 10 min before the image acquisition. The drug treatment was conducted under the 37°C and 5% CO_2 humidified atmosphere using a stage top incubator (TOKAI HIT).

The traction stress field in the PAAm gel substrate was calculated using the Fiji plugins, iterative PIV and Fourier transform traction cytometry (FTTC).[101] In brief, the displacement field in the gel substrate was obtained by the PIV analysis of fluorescence images of beads before and after cell detachment. From the displacement field, the traction stress field was reconstructed using the Fourier transform traction cytometry (FTTC) method.

Immunofluorescence

Immunostaining of cells was carried out as described previously.[56] Cells were fixed and permeabilized for 30 min with 4% formaldehyde and 0.2% Triton X-100 in the cytoskeletal stabilizing (CS) buffer.[102] This was followed by blocking with 1% BSA in CS buffer for 30 min. The cells were then incubated with primary antibodies for 40 min, washed, and further incubated with secondary antibodies for 40 min. Antibodies were diluted in CS buffer containing 1% BSA. The stained cells were observed with either a confocal microscope equipped with a 60x oil-immersion objective lens (NA 1.49, Nikon) or an epifluorescence microscope (BZ-710 or BZ-810, Keyence) equipped with a 100x oil-immersion objective lens (NA 1.30, Nikon or NA 1.40, Nikon).

Western blotting

Cells were collected and lysed with 2× lithium dodecyl sulfate sample buffer (Invitrogen) containing 2.5% β-mercaptoethanol. Proteins were separated by sodium dodecyl sulfate polyacrylamide gel electrophoresis (SDS-PAGE) (4–12% Bis-Tris gel; Invitrogen) and transferred onto a polyvinylidene fluoride membrane (Immobilon-P, Merck-Millipore). After incubation with primary antibodies followed by the secondary HRP-linked anti-mouse or HRP-linked anti-rabbit antibody (Cell Signaling Technology), immuno-reactive bands were visualized using SuperSignal West Femto Maximum Sensitivity Substrate (Thermo Fisher Scientific). Images were acquired by using a CCD Camera (Cool SNAP fx, Photometrics).

Measurement of Feret diameters of FAs

Feret diameters of FAs were measured in vinculin immunofluorescence images. After thresholding the vinculin images, individual FAs were selected manually. FAs contacting to neighboring ones were excluded from the analysis. Feret diameters of the selected FAs were measured using the Fiji software with the plugin, Measurements.

Quantification of cell area and cell shape

In phase contrast images of cells, cell area measurement and ellipse fitting of the cell shape were conducted using the Fiji software. Cell outline was traced manually, and ellipse fitting was carried out using the Fit Ellipse plugin. Ellipse perimeter was calculated as follows:

$$L = \pi(a+b)\left(1+\frac{3\left(\frac{a-b}{a+b}\right)^2}{10+\sqrt{4-3\left(\frac{a-b}{a+b}\right)^2}}\right) \quad \text{(Equation 1)}$$

where a and b are long and short diameters of an ellipse, respectively. To evaluate cell shape quantitatively, the ratio of cell outline against ellipse parameter was calculated.

Sigle cell migration assay

C2C12 cells were sparsely seeded onto fibronectin-coated glass bottom dish or 2.3 kPa PAAm gel substrates and grown overnight. Migrating cells were observed using the BioStation IM microscope (Nikon) under the 37°C and 5% CO_2 humidified atmosphere. Phase contrast images were acquired at 10-min intervals for up to 240 min. Individual cells were tracked using the Fiji plugin, Manual Tracking; we manually tracked the center of nuclei in phase contrast images. Persistence of cell migration was calculated by dividing the end-to-end distance of cell displacement during 120-240 min observation by the total length of the cell migration path. Cells that underwent mitosis during the observation were excluded from the analysis.

Wound healing assay

3.0×10^4 C2C12 cells were seeded onto the fibronectin-coated 96 well plate (Corning) and grown for 16 h. Formed cell monolayers were wounded using the 96-pin woundmaking tool (WoundMaker, Essen Bioscience). Each wound was 750 μm (± 20%) in width. The wound healing process was observed using the IncuCyte SX5 (Sartorius) under the 37°C and 5% CO_2 humidified atmosphere. Phase contrast images were acquired at 30-min intervals.

Actin polymerization assay

The stock solution of 100 μM rhodamine-conjugated actin protein (Cytoskeleton) was filtered (pore 0.22 μm; Millipore) and diluted to 0.4 μM concentration with the permeabilization buffer (CS buffer supplemented with 0.03% digitonin and the protease inhibitor cocktail (Sigma)), just before use. Cells were incubated with the diluted actin solution for 1 min at room temperature. After the incubation, cells were fixed with 3.7% formaldehyde, permeabilized with 0.2% Triton X-100, blocked with 1% BSA, and subjected to immunostaining in CS buffer.

FRAP analysis

Fluorescence recovery after photobleaching (FRAP) experiments were carried out using the A1Rsi confocal microscope (Nikon). SFs in C2C12 cells expressing GFP-tagged actin were locally photobleached with 405 nm laser for 0.5 sec with 100 % of the laser power (the size of bleached area was 1.6 x 3.6 μm), and fluorescence images were acquired every 0.5 sec for 1 min with 3%-10% of the laser power. Photobleach outside the region of interest (ROI) during the observation was negligible. For the analysis of fluorescence intensity, the NIS-Elements AR software (Nikon) was used. The relative fluorescence intensities in ROI were plotted against time, and the plots were fitted with Equation 2,

$$I(t) / I_0 = M\left[1 - \exp(-t/\tau)\right] + c \qquad \text{(Equation 2)}$$

where $I(t)$ and I_0 represent the mean fluorescence intensities in ROI at time t and before photobleaching, respectively, and the mobile fraction (M), the time constant (τ) and the constant (c) were used as fitting parameters.[103] Time zero was set as the time point when photobleaching was conducted. The half-recovery time $T_{1/2}$ was calculated as,

$$T_{1/2} = ln(2) \times \tau \qquad \text{(Equation 3)}$$

Atomic force microscopy (AFM)

AFM measurements were performed using NanoWizard IV AFM (JPK Instruments-AG, Bruker) mounted on top of an inverted optical microscope (IX73, Olympus, Japan) equipped with a digital CMOS camera (Zyla, Andor) as previously described.[43] The AFM quantitative imaging (QI) mode was then used to obtain force-displacement curves at the mid-region of the cell surfaces (128 × 128 points, 20 μm × 20 μm of measured area), using a precisely controlled indentation test using silicon nitride cantilevers with a cone probe (BioLever-mini, BL-AC40TS-C2, Olympus) at a spring constant of 0.071–0.074 N/m. The QI mode measurements were carried out within 40 min after the transfer of the specimen cells to the AFM at room temperature (25°C). To determine the elastic modulus (*i.e.*, the Young's modulus) the force-displacement curves were fitted to the Hertz contact model:

$$F = \frac{2E \cdot \tan\alpha}{\pi(1 - \nu^2)}\delta^2 \qquad \text{(Equation 4)}$$

where F is the applied force, E is the elastic modulus, ν is the Poisson's ratio (0.5 for a non-compressible biological sample), α is the opening angle of the cone of the cantilever tip, and δ is the indentation depth of the cells. We calculated the elastic modulus at each point and produced elastic modulus maps of the specimen cells. To examine colocalization of the elastic modulus with SFs, we conducted elasticity mapping by AFM in living cells in which the actin cytoskeleton was labeled with the carboxylated silicon–rhodamine (SiR)-actin live cell imaging probe (Cytoskeleton).

Modeling and numerical simulation

To analyze effects of myosin II and α-actinin on SF dynamics, we developed a simple mathematical model based on molecular behaviors in a bottom-up manner, involving movement and turnover of actin filaments, myosin II-generated contractile force, and crosslinking by α-actinin. Using this model, we performed numerical simulations and analyzed flow velocity of actin filaments and traction force acting on FAs. In this model, we consider a SF with the total length of L_{SF}. For simplification, the distribution of actin filaments along the SF, represented by the x-axis, was considered by applying a one-dimensional continuum approximation. In this assumption, the cross-sectional alignment within the SF and the alignment of individual filaments along the SF are ignored.

First, the distribution of actin filaments was considered. For simplification, the lengths of all filaments are regarded as uniform, denoted by L. The line density and flow velocity of the filament having its center of

gravity at position x are denoted by ρ and v, respectively. The number of filaments passing through position x, represented by n (x), is given by

$$n(x) = \int_{-L/2}^{L/2} \rho(x+y)dy. \quad \text{(Equation 5)}$$

Second, myosin II-generated contractile force between filaments was introduced. Let λ_{MY} be the line density of myosin binding to filaments and let χL simply be the contractile force generated by a binding myosin acting on a filament. The pressure in the SF at position x, represented by P (x), is given by

$$P(x) = -n(x)\lambda_{MY}\chi L. \quad \text{(Equation 6)}$$

The ratio of the filaments having their center of gravity at position x to all filaments passing through the small region dy near position y is given by $\rho(x)dy/n(y)$. Assuming that the force applied to the cross-section of the SF is equally applied to all filaments passing through the cross-section, the force acting on the filaments with center of gravity at position x in the small region dy near position y is given by $(\rho(x)dy/n(y))(\partial P(y)/\partial y)$. Therefore, the summation force per unit length acting on the filaments with center of gravity at position x, represented by S (x), is given by

$$S(x) = \int_{x-L/2}^{x+L/2} \frac{\rho(x)}{n(y)} \frac{\partial P(y)}{\partial y} dy. \quad \text{(Equation 7)}$$

Third, effects of crosslinking by α-actinin between actin filaments were introduced. By denoting the line density of α-actinin binding to filaments by λ_{AA}, the spring constant by K, and the dissociation constant by k_{off}^{AA}, the frictional force acting on a unit length of actin filament can be written as $\lambda_{AA}K\Delta v/k_{off}^{AA}$, where Δv is the relative velocity to the surroundings.[104] By considering the velocities of the filaments with centers of gravity at positions x and y, represented by $v(x)$ and $v(y)$, respectively, the frictional force acting between two filaments with velocities $v(x)$ and $v(y)$, represented by $\gamma(x,y)$, is written by

$$\gamma(x,y) = \frac{\lambda_{AA}K(v(x)-v(y))}{k_{off}^{AA}}(L-|x-y|). \quad \text{(Equation 8)}$$

Therefore, the α-actinin-generated frictional force acting on a unit length of the filament with center of gravity at position x from the surrounding filaments, represented by $\Gamma(x)$, is given by

$$\Gamma(x) = \int_{x-L}^{x+L} \rho(x)\rho(y)\gamma(x,y)dy. \quad \text{(Equation 9)}$$

Fourth, the force balance on the SF at position x is given by

$$0 = S(x) - \rho(x)\xi Lv(x) - \Gamma(x), \quad \text{(Equation 10)}$$

where the first, second, and third terms indicate the myosin II-generated force, frictional force to the surrounding medium, and α-actinin-generated frictional force. In the second term, ξ is the friction per unit length between actin filaments and surroundings. Using Equations (5), (6), (7), (8), and (9), Equation 10 can be rewritten by

$$0 = \int_{x-L/2}^{x+L/2} \frac{\rho(x)}{n(y)} \frac{\partial P(y)}{\partial y} dy - \rho(x)\xi Lv - \int_{x-\frac{L}{2}}^{x+\frac{L}{2}} \rho(x)\rho(y)\left(\frac{\lambda_{AA}K(v(x)-v(y))}{k_{off}^{AA}}\right)dy. \quad \text{(Equation 11)}$$

Fifth, conservation of actin filaments within the SF was considered. The number of actin filaments in the SF can be varied by turnover via polymerization and depolymerization as well as flux along the SF. The density conservation of actin filaments in the SF is written by

$$\frac{\partial \rho}{\partial t} = \frac{\rho_0 - \rho}{\tau^{AF}} - \frac{\partial(\rho v)}{\partial x} \quad \text{(Equation 12)}$$

where the first and second terms indicate the turnover and flux, respectively.[105] In the first term, ρ_0 and τ^{AF} indicate the line density of filaments in the SF under equilibrium and the characteristic time of turnover, respectively.

Lastly, initial and boundary conditions were introduced. One of the steady-state solutions of Equations (11) and (12) is $\rho = \rho_0$, i.e., filaments are homogenously distributed along the SF. Using ρ_0, the initial condition was given by

$$\rho = \rho_0 + w, \quad \text{(Equation 13)}$$

where w is a noise with mean 0 and standard deviation $0.1\rho_0$. Moreover, assuming that the end regions of the SF were fixed on ECM through FAs, the fixed boundary conditions were applied to the end regions. Setting the end regions to $0 \le x \le L/2$ and $L_{SF} - L/2 \le x \le L_{SF}$ for simplification, boundary conditions were written by

$$v = 0 \quad \text{as} \quad 0 \le x \le \frac{L}{2}, L_{SF} - \frac{L}{2} \le x \le L_{SF}$$
$$\rho = \begin{cases} 0 & \text{as} \quad x < 0, L_{SF} < x \\ \rho_0 & \text{as} \quad 0 \le x \le \frac{L}{2}, L_{SF} - \frac{L}{2} \le x \le L_{SF} \end{cases} \quad \text{(Equation 14)}$$

To evaluate flow of actin filaments in the SF, the maximum velocity of filament flow in all filaments, represented by v_{max}, were calculated as follows.

$$v_{max} = \max_{0 \le x \le L_{SF}} |v(x)| \quad \text{(Equation 15)}$$

Moreover, to evaluate traction force acting on FAs, total force acting on the region of $0 \le x \le L/2$ was calculated as follows.

$$F_{trc} = \int_0^{\frac{L}{2}} (S - \Gamma) dx \quad \text{(Equation 16)}$$

To perform numerical simulations, the equations and parameters were nondimensionalized by introducing the unit number of filaments, $\rho_0 L$, unit length, L, unit time, τ^{AF}, and unit force, $\xi L^2/\tau^{AF}$. By considering the average length of each sarcomeric unit experimentally measured from periodic distribution of α-actinin,[106] the total length of the SF was set to $L_{SF} = 10L$. Values of the control parameters, $\lambda_{MY}\chi$ and $\lambda_{AA}K/k_{off}^{AA}$, were explored. Numerical simulations were performed with second-order accuracy using the Euler method with $\Delta t = 10^{-6}\tau^{AF}$. The simulations were performed during $10\tau^{AF}$, sufficient period to reach steady state, and statistical values of Equations (15) and (16) were calculated during the last τ^{AF}.

QUANTIFICATION AND STATISTICAL ANALYSIS

All statistical analysis were carried out using the Origin Pro software (OriginLab). For two-sample comparisons, Student's *t* test or Welch's *t* test was used after *F*-test. For multi-sample comparisons, Tukey test was used. Statistical significance was accepted if $p < 0.05$. Pooled data were presented as the mean ± standard error of the mean (SEM), or as data dots with the mean.